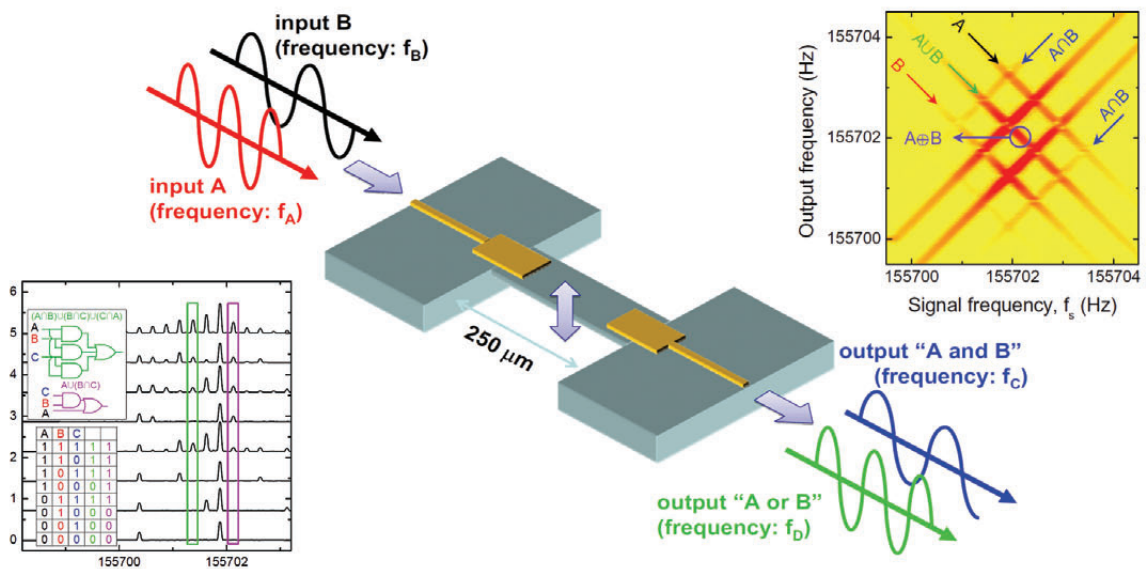


Research Activities in NTT Basic Research Laboratories

Volume 21
Fiscal 2010

July 2011

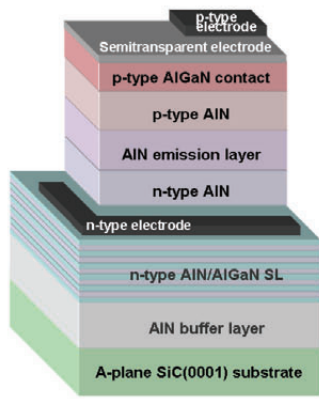
NTT Basic Research Laboratories,
Nippon Telegraph and Telephone Corporation (NTT)
<http://www.brl.ntt.co.jp/>



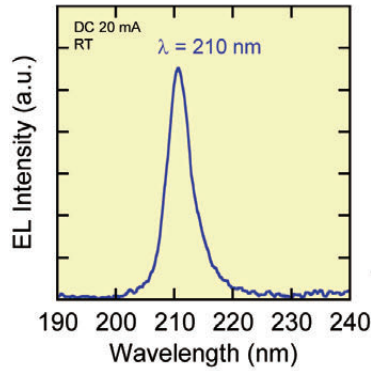
Cover photograph:

Parametric Frequency Conversion and Logic Operations Using Electromechanical Resonators

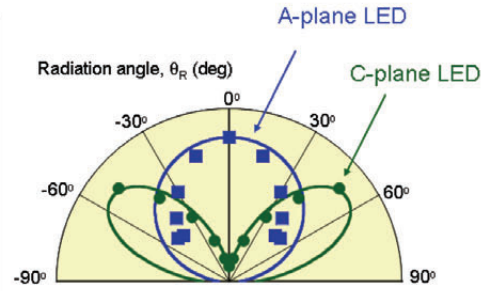
We realize a logic device in an electromechanical resonator. Two inputs, A and B, are applied to one electrode as alternate voltage of different frequencies, f_A and f_B , respectively. The signals are transferred to mechanical oscillations which are mixed and frequency converted to f_C and f_D . These two outputs are obtained when both (for f_C) or just one (for f_D) of the inputs are active which corresponds to logicals (A and B) and (A or B) respectively. Other examples of multiple logic operation are also shown. (Page 27)



A-plane AlN LED



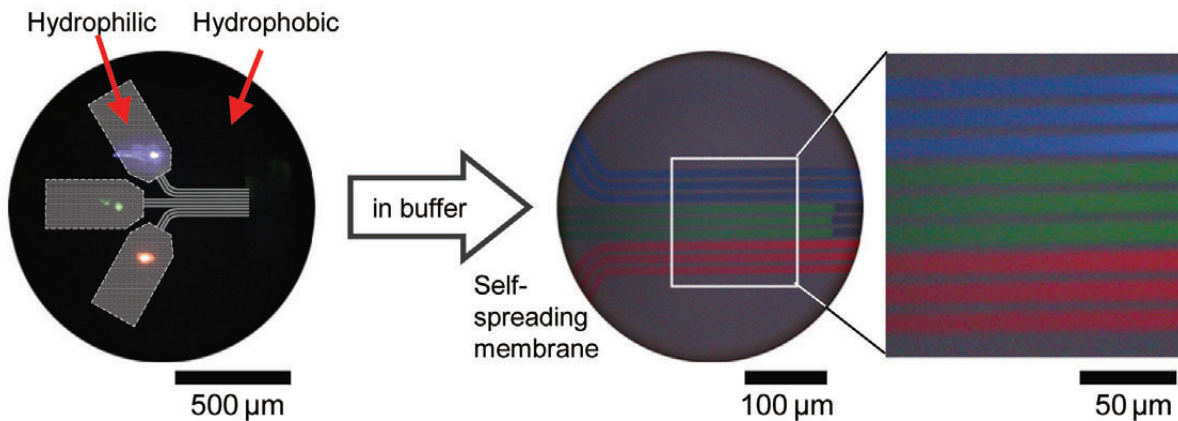
Emission spectrum of A-plane AlN LED



Radiation properties of A-plane and C-plane LED

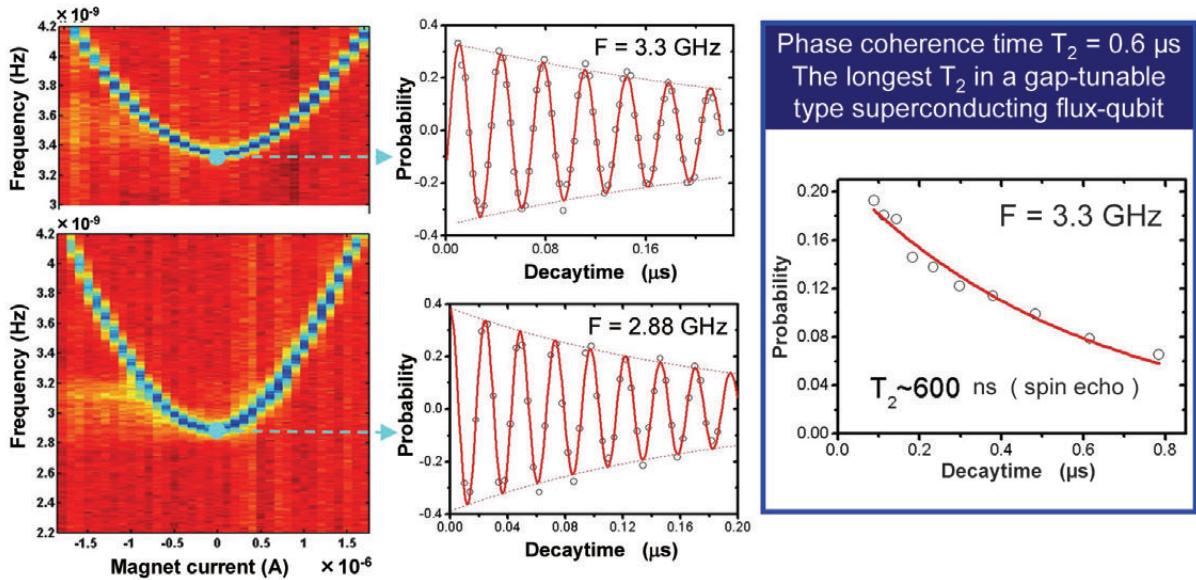
Emission Mechanism of AlN Deep-Ultraviolet Light-Emitting Diode

We have developed an aluminum nitride (AlN) deep-ultraviolet light-emitting diode (LED) with a wavelength of 210 nm, which is the shortest wavelength ever observed from any semiconductor. Due to a unique valence band structure (negative crystal-field splitting energy), AlN has a strong polarization property and therefore its emission intensity largely changes depending on the crystal planes of its surface. Here, for improving the AlN LED's emission efficiency, we propose an A-plane LED structure, which shows strong surface emission compared with the conventional C-plane one. (Page 16)



Highly Integrative Artificial Cell Membrane Microarray

We develop a new technique for fabricating an artificial cell membrane microarray, which is an important platform for biochip applications. Parallel 10- μ m-wide lines, each filled with a membrane with a unique composition at 5- μ m intervals are successfully fabricated. The red, green and blue fluorescence correspond to the different membrane compositions. Our new method offers a finer microarray that is more than 100 times more highly integrated, than those obtained with previously reported methods. (Page 18)

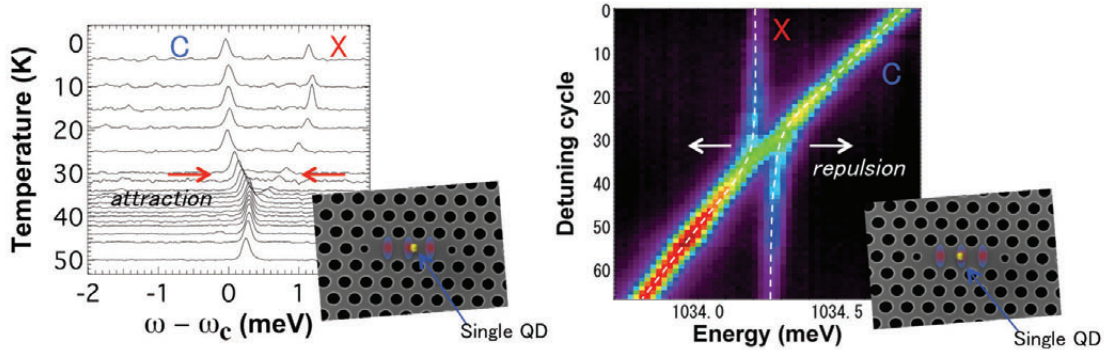


Ramsey fringes at different operating frequencies

Dephasing time obtained by spin-echo

Coherent Operation of a Gap-Tunable Flux Qubit

By replacing the smallest Josephson junction of the qubit with a DC-SQUID, we demonstrate the *in situ* coherent tunability of the gap of a superconducting flux qubit. In a conventional design, the tunneling energy of the flux-qubit is fixed in the fabrication process. However, in the new device, we can control qubit tunneling energy in nano second while keeping the qubit at its degeneracy point (optimum flux bias) where the flux-noise is considered to be minimum. From Ramsey fringes and echo-measurement, the best dephasing time of $T_2=0.6 \mu\text{s}$ in this type of flux-qubit are obtained. This improved device will accelerate research of quantum information processing via quantum bus and quantum memory. (Page 31)



PL spectra in a weak coupling regime (mode attraction).

PL color map in a strong coupling regime (disappearance of Rabi splitting with anti-crossing dispersion).

Cavity Quantum Electrodynamics Using Single Quantum Dot

We fabricate a photonic crystal nanocavity with a single quantum dot (QD), and investigate the interaction between a single exciton (X) and the cavity mode (C), namely the effect of cavity quantum electrodynamics (cQED). In a weak X-C coupling regime, we observe an unusual mode attraction between X and C. Moreover, we find that Rabi splitting disappears while anti-crossing dispersion is maintained in a strong coupling regime. These are novel cQED effects that arise from the large exciton dephasing of the solid-state two-level system. (Page 39)

Message from the Director



We are extremely grateful for your interest and support with respect to our research activities.

The three research areas at NTT Basic Research Laboratories (NTT-BRL), namely Materials Science, Physical Science, and Optical Science, are undertaking work designed to create new values supporting NTT's future business and to promote advances in science that will ultimately benefit all mankind.

A fundamental goal of these research activities is to improve global competitiveness. Therefore, NTT-BRL is collaborating with many universities and research institutes throughout the world as well as with other NTT laboratories. NTT-BRL organizes international conferences related to quantum physics and nanotechnology and also holds a "Science Plaza" to enhance public understanding of our activities and to ensure a frank exchange of opinions.

It gives us immense pleasure to fulfill our mission of being an open laboratory, and to disseminate our research output worldwide. Your continued support is greatly appreciated.

June, 2011

Itaru Yokohama
Director
NTT Basic Research Laboratories

Contents

page

◆ Cover	
◆ Parametric Frequency Conversion and Logic Operations Using Electromechanical Resonators	
◆ Color Frontispiece	I
◆ Emission Mechanism of AlN Deep-Ultraviolet Light-Emitting Diode	
◆ Highly Integrative Artificial Cell Membrane Microarray	
◆ Coherent Operation of a Gap-Tunable Flux Qubit	
◆ Cavity Quantum Electrodynamics Using Single Quantum Dot	
◆ Message from the Director	III
◆ NTT Basic Research Laboratories Organogram	1
◆ Member List	2

I. Research Topics

◇ Overview of Research in Laboratories	13
◇ Materials Science Laboratory	14
◆ Robust Superconductivity in Pr ₂ CuO ₄ Prepared by MBE	
◆ Nucleus and Spiral Growth Mechanisms of GaN Studied by Selective-Area MOVPE	
◆ Emission Mechanism of AlN Deep-Ultraviolet Light-Emitting Diode	
◆ AlGaIn/GaN HEMTs Epitaxially Grown on Single-Crystal Diamond	
◆ Highly Integrative Artificial Cell Membrane Microarray	
◆ Evaluation of Carrier Density in Doped Single-Wall Carbon Nanotubes	
◆ Transport Properties of Epitaxial Monolayer and Bilayer Graphene	
◆ Manipulation of Biomolecules on Solid Substrate Using Artificial Cell Membrane	
◆ AFM Observation of a Receptor Subunit Structure	
◆ Electrostatic Control of Artificial Cell Membrane Self-Spreading	
◇ Physical Science Laboratory	24
◆ Single-Electron Resonant Activation over an Oscillating Barrier	
◆ Theoretical Study of Magnetoelectric and Thermoelectric Properties of Graphene	
◆ Strong Stark Effect in Electroluminescence from Phosphorous-Doped SOI-MOSFETs	
◆ Parametric Frequency Conversion and Logic Operations Using Electromechanical Resonators	
◆ Carrier-Mediated Opto-Mechanical Coupling in GaAs Cantilevers	

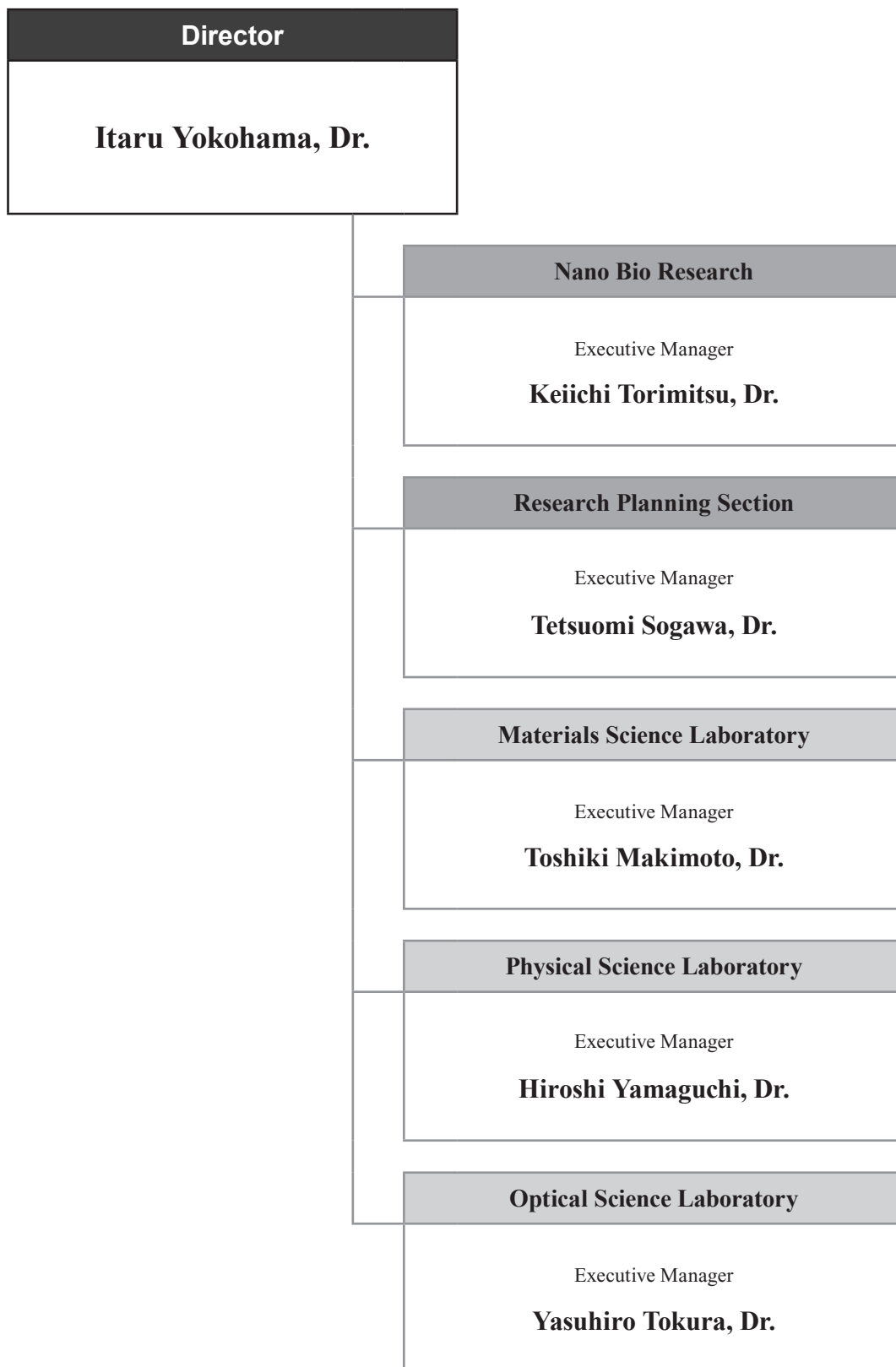
◆ Voltage-Controlled Group Velocity of Edge Magnetoplasmon in the Quantum Hall Regime	
◆ Wide-Band Capacitance Measurement on a Semiconductor Double Quantum Dot for Studying Tunneling Dynamics	
◆ Coherent Operation of a Gap-Tunable Flux Qubit	
◆ Generation of Non-Classical Microwave Photon States in an Inductor-Capacitor Resonator Coupled to a Superconducting Flux Qubit	
◆ Quantum Zeno Effect with a Superconducting Qubit	
◆ Evaluation of Spin Polarization in $p\text{-In}_{0.96}\text{Mn}_{0.04}\text{As}$ Using Andreev Reflection Spectroscopy Including Inverse Proximity Effect	
◆ Photoluminescence Spectroscopy of the Low-Density Two-Dimensional Electron System in Electric Fields	
◇ Optical Science Laboratory	36
◆ Single-Photon Detection Using Magnesium Diboride Superconducting Nanowire at Telecommunication Wavelength	
◆ Tokyo QKD Network	
◆ Kondo Effects and Current Shot Noise in a Double Quantum Dot	
◆ Cavity Quantum Electrodynamics Using Single Quantum Dot	
◆ Nanowires Laterally Grown on GaAs Substrates in the Vapor-Liquid-Solid Mode	
◆ Coherent Phonons in Metallic Single-Walled Carbon Nanotubes	
◆ High- Q One-Dimensional Photonic Crystal Nanocavity in a Silicon/SOI Platform	
◆ GPGPU Acceleration of the FDTD Calculation	

II. Data

◇ Science Plaza 2010	45
◇ International Symposium on Nanoscale Transport and Technology (ISNTT2011)	46
◇ The 6th Advisory Board (Fiscal 2010)	47
◇ Award Winners' List (Fiscal 2010)	48
◇ In-house Award Winners' List (Fiscal 2010)	49
◇ Numbers of Papers, Presentations and Patents (2010)	50
◇ List of Invited Talks at International Conferences (2010)	52

NTT Basic Research Laboratories Organogram

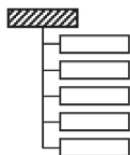
As of March 31, 2011



Member List

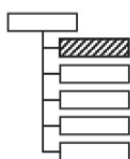
As of March 31, 2011
(* / left the position in a year)

NTT Basic Research Laboratories



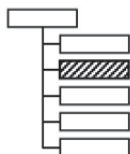
Director, **Dr. Itaru Yokohama**

Nano Bio Research



Executive Manager, **Dr. Keiichi Torimitsu**

Research Planning Section



Executive Research Scientist, **Dr. Tetsuomi Sogawa**

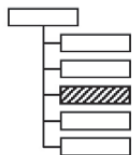
Senior Research Scientist, Dr. Hiroki Takesue
Dr. Kazuhide Kumakura*

Senior Research Scientist, Dr. Akihiko Shinya
Dr. Kazuaki Furukawa*

NTT Research Professor

Prof. Shintaro Nomura (University of Tsukuba) *
Prof. Kyo Inoue (Osaka University) *

Materials Science Laboratory



Executive Manager, **Dr. Toshiki Makimoto**

Dr. Nahoko Kasai
Dr. Satoru Suzuki*

Thin-Film Materials Research Group:

Dr. Hideki Yamamoto (Group Leader)

Dr. Makoto Kasu*

Dr. Makoto Kasu

Dr. Hisashi Sato

Dr. Yoshitaka Taniyasu

Dr. Yasuyuki Kobayashi

Dr. Tetsuya Akasaka

Dr. Yoshiharu Krockenberger

Dr. Hideki Yamamoto*

Dr. Kazuhide Kumakura

Dr. Kazuyuki Hirama

Low-Dimensional Nanomaterials Research Group:

Dr. Hiroki Hibino (Group Leader)

Dr. Fumihiko Maeda

Dr. Satoru Suzuki

Dr. Kazuaki Furukawa

Dr. Kenichi Kanzaki

Dr. Hiroo Omi

Shinichi Tanabe

Molecular and Bio Science Research Group:

Dr. Keiichi Torimitsu (Group Leader)

Dr. Koji Sumitomo

Dr. Hiroshi Nakashima

Dr. Youichi Shinozaki*

Dr. Nahoko Kasai*

Dr. Yoshiaki Kashimura

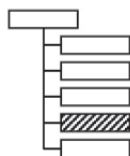
Dr. Aya Tanaka

Dr. Akiyoshi Shimada

Touichiro Goto

Dr. Shogo Tsukada

Physical Science Laboratory



Executive Manager, **Dr. Hiroshi Yamaguchi**

Toru Yamaguchi
Dr. Kenji Yamazaki*

Takeshi Karasawa

Nanodevices Research Group:

Dr. Akira Fujiwara (Group Leader)

Dr. Yukinori Ono

Dr. Jin-ichiro Noborisaka

Dr. Hiroyuki Kageshima

Dr. Gento Yamahata

Dr. Katsuhiko Nishiguchi

Dr. Gabriel Lansbergen

Nanostructure Technology Research Group:

Dr. Hiroshi Yamaguchi (Group Leader)

Dr. Kenji Yamazaki

Dr. Hajime Okamoto

Junzo Hayashi

Toru Yamaguchi*

Daiki Hatanaka

Dr. Koji Onomitsu

Dr. Imran Mahboob

Quantum Solid State Physics Research Group:

Dr. Koji Muraki (Group Leader)

Dr. Kiyoshi Kanisawa

Dr. Toshiaki Hayashi

Dr. Ken-ichi Hitachi

Tadashi Saku

Dr. Satoshi Sasaki

Dr. Takeshi Ohta

Dr. Keiko Takase

Dr. Kyoichi Suzuki

Dr. Norio Kumada

Dr. Gerardo Gamez*

Superconducting Quantum Physics Research Group:

Dr. Kouichi Semba (Group Leader)

Dr. Hayato Nakano

Hiroataka Tanaka

Dr. Xiaobo Zhu

Dr. Shiro Saito

Dr. Kousuke Kakuyanagi

Dr. Shin-ichi Karimoto

Dr. Alexandre Kemp

Spintronics Research Group:

Dr. Tatsushi Akazaki (Group Leader)

Dr. Yuichi Harada

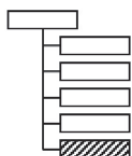
Dr. Yoshiaki Sekine

Dr. Hiroyuki Tamura

Dr. Hiroshi Irie

Dr. Masumi Yamaguchi

Optical Science Laboratory



Executive Manager, **Dr. Yasuhiro Tokura**

Dr. Takehiko Tawara
Dr. Satoshi Sasaki*

Quantum Optical State Control Research Group:

Dr. Yasuhiro Tokura (Group Leader)

Dr. Kaoru Shimizu	Kazuhiro Igeta	Dr. Masami Kumagai
Dr. Makoto Yamashita	Dr. Hiroyuki Shibata	Dr. Hiroki Takesue*
Dr. Tetsuya Mukai	Dr. Toshimori Honjo	Dr. Fumiaki Morikoshi
Dr. Kiyoshi Tamaki	Daisuke Hashimoto	Dr. Koji Azuma
Dr. Nobuyuki Matsuda	Dr. William John Munro	Dr. Kensuke Inaba
Dr. Toshihiro Kubo		

Quantum Optical Physics Research Group:

Dr. Tetsuomi Sogawa (Group Leader)

Dr. Hidetoshi Nakano	Dr. Tadashi Nishikawa	Dr. Hideki Gotoh
Hidehiko Kamada	Dr. Kouta Tateno	Dr. Takehiko Tawara*
Dr. Katsuya Oguri	Dr. Atsushi Ishizawa	Dr. Haruki Sanada
Dr. Guoquiang Zhang	Dr. Keiko Kato	

Photonic Nano-Structure Research Group:

Dr. Masaya Notomi (Group Leader)

Dr. Atsushi Yokoo	Dr. Eiichi Kuramochi	Dr. Akihiko Shinya*
Dr. Hideaki Taniyama	Dr. Hisashi Sumikura	Dr. Kengo Nozaki
Dr. Young-Geun Roh*	Dr. Jimyung Kim	Dr. Danang Birowosuto

Senior Distinguished Researcher



Masaya Notomi was born in Kumamoto, Japan, on 16 February 1964. He received his B.E., M.E., and Ph. D. degrees in applied physics from University of Tokyo, Japan in 1986, 1988, and 1997, respectively. In 1988, he joined NTT Optoelectronics Laboratories. Since then, his research interest has been to control the optical properties of materials and devices by using artificial nanostructures, and engaged in research on quantum wires/dots and photonic crystal structures. He has been in NTT Basic Research Laboratories since 1999, and a group leader of Photonic Nanostructure Research Group since 2004. He is also entitled as Senior Distinguished Scientist of NTT. From 1996-1997, he was with Linköping University in Sweden as a visiting researcher. He was a guest associate professor of Department of Applied Electronics in Tokyo Institute of Technology (2003-2009), and is currently a guest professor of Department of Physics in Tokyo Institute of Technology. He received IEEE/LEOS Distinguished Lecturer Award in 2006, JSPS (Japan Society for the Promotion of Science) prize in 2009, Japan Academy Medal in 2009, and The Commendation for Science and Technology by the Minister of Education, Culture, Sports, Science and Technology (Prize for Science and Technology, Research Category) in 2010. He is serving as a member of National University Corporation Evaluation Committee in the Japanese government. He is also a member of the Japan Society of Applied Physics, APS, IEEE, and OSA.

Distinguished Researchers



Akira Fujiwara was born in Tokyo, Japan on March 9, 1967. He received his B.S., M.S., and Ph.D. degrees in applied physics from The University of Tokyo, Japan in 1989, 1991, and 1994, respectively. In 1994, he joined NTT LSI Laboratories and moved to NTT Basic Research Laboratories in 1996. Since 1994, he has been engaged in research on silicon nanostructures and their application to single-electron devices. He was a guest researcher at the National Institute of Standards and Technology (NIST), Gaithersburg, MD, USA during 2003-2004. He received the SSDM Young Researcher Award in 1998, SSDM Paper Award in 1999, and Japanese Journal of Applied Physics (JJAP) Paper Awards in 2003 and 2006. He was awarded the Young Scientist Award from the Minister of MEXT (Ministry of Education, Culture, Sports, Science, and Technology) in 2006. He is a member of the Japan Society of Applied Physics and the IEEE.



Koji Muraki was born in Tokyo, Japan in 1965. He received his B.S., M.S., and Ph.D. degrees in applied physics from The University of Tokyo, Japan, in 1989, 1991, and 1994, respectively. In 1994, he joined NTT Basic Research Laboratories, Kanagawa, Japan. Since then, he has been engaged in the growth of high-mobility heterostructures and the study of highly correlated electronic states realized in such structures. He was a guest researcher at Max-Planck Institute, Stuttgart, Germany during 2001-2002. He is a member of the Physical Society of Japan and Japan Society of Applied Physics.



Hiroshi Yamaguchi was born in Osaka on October 30, 1961. He received the B.E., M.S. in physics and Ph.D. degrees in engineering from the Osaka University in 1984, 1986 and 1993, respectively. He joined NTT Basic Research Laboratories in 1986 and has engaged in the study of compound semiconductor surfaces using electron diffraction and scanning tunneling microscopy. His current interests are micro/nanomechanical devices using semiconductor heterostructures. He was a visiting research fellow in Imperial College, University of London, U.K. during 1995-1996 and a visiting research staff in Paul Drude Institute, Germany in 2003. He is a guest professor in Tohoku University from 2006 and a director of the Japanese Society of Applied Physics in 2008 and 2009. He is currently an executive manager of Physical Science Laboratory and a group leader of Nanostructure Technology Research Group. He is a member of the Japan Society of Applied Physics and the Physical Society of Japan.



Yoshitaka Taniyasu was born in Toyama, Japan on June 10, 1973. He received his B.E., M.E., and Dr. Eng. degrees in electrical engineering from Chiba University, Chiba, Japan in 1996, 1998, and 2001, respectively. He joined NTT Basic Research Laboratories in 2001. He has been engaged in wide bandgap semiconductor research. His current interests are epitaxial growth and device application of nitride semiconductors, especially aluminum nitride (AlN). He received the Young Scientist Award for the Presentation of the Excellent Paper at the Japan Society of Applied Physics (JSAP) in 2001, the Young Scientist Award at the Semiconducting and Insulating Materials Conference in 2007, and the Young Scientists' Prize from the Minister of Education, Culture, Sports, Science and Technology in 2011. He is a member of the JSAP.



Norio Kumada was born in Gifu, Japan in 1975. He received his B.S., M.S., and Ph.D. degrees in physics from Tohoku University, Japan, in 1998, 2000, and 2003, respectively. In 2003, he joined NTT Basic Research Laboratories, Kanagawa, Japan. Since then, he has been engaged in the study of highly correlated electronic states realized in semiconductor heterostructures. He received Young Scientist Award of the Physical Society of Japan in 2008. He is a member of the Physical Society of Japan.

Advisory Board (2010 Fiscal Year)

Name	Affiliation
Prof. Gerhard Abstreiter	Walter Schottky Institute, Germany
Prof. Boris L. Altshuler	Department of Physics, Columbia University, U.S.A.
Prof. Serge Haroche	Département de Physique, De l'Ecole Normale Supérieure, France
Prof. Theodor W. Hänsch	Max-Planck-Institut für Quantenoptik, Germany
Prof. Mats Jonson	Department of Physics, Göteborg University, Sweden
Prof. Anthony J. Leggett	Department of Physics, University of Illinois at Urbana-Champaign, U.S.A.
Prof. Johan E. Mooij	Kavli Institute of Nanoscience, Delft University of Technology, The Netherlands
Prof. John F. Ryan	Clarendon Laboratory, University of Oxford, U.K.
Prof. Klaus von Klitzing	Max-Planck-Institut für Festkörperforschung, Germany

Invited / Guest Scientists (2010 Fiscal Year)

Name	Affiliation	Period
Dr. Hideomi Hashiba	Institute of Quantum Science, Nihon University	Apr. 2010 – Mar. 2011
Dr. Lars Tiemann	Japan Science and Technology Agency (JST)	Apr. 2010 – Mar. 2011
Dr. Takasumi Tanabe	Dept. of Electronics and Electrical Engineering, Keio University	Apr. 2010 – Mar. 2011
Prof. David Cox	University of Surrey, U.K.	Apr. 2010 – Jun. 2010
Prof. Tobias Nyberg	Royal Institute of Technology, Sweden	Jul. 2010 – Aug. 2010
Ms. Katherine Brown	University of Leeds, U. K.	Sep. 2010
Dr. Stefan Fölsch	Paul-Drud-Institute, Germany	Oct. 2010
Prof. Johan Elisa Mooij	Delft University of Technology, The Netherlands	Oct. 2010 – Nov. 2010
Prof. Yuli V. Nazarov	Delft University of Technology, The Netherlands	Nov. 2010
Prof. Amnon Aharony	Ben Gurion University of the Negev, Israel	Jan. 2011 – Feb. 2011
Prof. Ora Entin-Wohlman	Ben Gurion University of the Negev, Israel	Jan. 2011 – Feb. 2011
Dr. Daniel Paul Collins	University of Oxford, U. K.	Jan. 2011 – Feb. 2011
Dr. Akiko Ueda	Ben Gurion University, Israel	Jan. 2011 – Feb. 2011
Dr. Genki Odawara	Applied Physics Curriculum1, Waseda University School of Advanced Science and Engineering	Feb. 2011 – Mar. 2011

Overseas Trainees (2010 Fiscal Year)

Name	Affiliation	Period
Oliver Johan Pirquet	University of Victoria, Canada	Sep. 2009 – Apr. 2010
Jessica Sparks	University of Waterloo, Canada	Sep. 2009 – Apr. 2010
Arianne McAllister	University of Ottawa, Canada	Sep. 2009 – Aug. 2010
Fabio Massimo Zennaro	Polytecnico di Milano, Italy	Jan. 2010 – Aug. 2010
Gary Wolfowicz	Ecole Normale Supérieure (ENS) de Cachan, France	Jan. 2010 – Aug. 2010
David Framil Carpeno	Complutense Univeristy of Madrid, Spain	Jan. 2010 – Aug. 2010
Jan Fiala	Czech Technical University in Prague, Czech Republic	Jan. 2010 – Aug. 2010
Juan Manuel Agudo Carrizo	Polytechnic University of Valencia (UPV), Spain	Jan. 2010 – Aug. 2010
Romain Duval	INSA (Institut National des Sciences Appliquées de Toulouse), France	Feb. 2010 – Aug. 2010
Kylie Ellis	The University of Adelaide, Australia	Mar. 2010 – Apr. 2010
Yuichiro Matsuzaki	University of Oxford, U.K.	Mar. 2010 – Apr. 2010
Shaun Lee	University of British Columbia, Canada	May. 2010 – Dec. 2010
Nadege Kaina	ESPCI (Ecole Supérieure de Physique et de Chimie Industrielle), France	July. 2010 – Dec. 2010
Quentin Wilmart	ESPCI (Ecole Supérieure de Physique et de Chimie Industrielle), France	July. 2010 – Dec. 2010
Antoine Gaume	ESPCI (Ecole Supérieure de Physique et de Chimie Industrielle), France	July. 2010 – Dec. 2010
Mohamed Oudah	University of Ottawa, Canada	Sep. 2010 – Sep. 2011
Yasir Makhdoom	University of British Columbia, Canada	Sep. 2010 – Sep. 2011
Jessica Planade	ESPCI (Ecole Supérieure de Physique et de Chimie Industrielle), France	Sep. 2010 – Dec. 2010
Jelena Baranovic	University of Oxford, U.K.	Nov. 2010 – Dec. 2010
Roberto Lo Nardo	Palermo University, Italy	Jan. 2011 – Aug. 2011
Diego Sabbagh	University of Studies "Roma Tre", Italy	Jan. 2011 – Aug. 2011
Bas van den Broek	Delft University of Technology, The Netherlands	Jan. 2011 – Mar. 2011
Yibo Fu	University of Toulouse, France	Feb. 2011 – Sep. 2011

Domestic Trainees (2010 Fiscal Year)

Name	Affiliation	Period
Kohei Morita	Kyushu University, Japan	Apr. 2010 – Mar. 2011
Shogo Aihara	Keio University, Japan	Apr. 2010 – Mar. 2011
Yasuhiko Oda	University of Tokyo, Japan	Apr. 2010 – Mar. 2011
Takayuki Watanabe	Tohoku University, Japan	Apr. 2010 – Mar. 2011
Tatsuki Takakura	University of Tokyo, Japan	Apr. 2010 – Mar. 2011
Hiroki Shioya	University of Tokyo, Japan	Apr. 2010 – Mar. 2011
Takashi Kobayashi	Tohoku University, Japan	Apr. 2010 – Mar. 2011
Yuma Okazaki	Tohoku University, Japan	Apr. 2010 – Mar. 2011
Ken-ichiro Kusudo	University of Tokyo, Japan	Apr. 2010 – Mar. 2011
Naoyuki Masumoto	University of Tokyo, Japan	Apr. 2010 – Mar. 2011
Hiroshi Kamata	Tokyo Institute of Technology, Japan	Apr. 2010 – Mar. 2011
Yu Morikawa	University of Tsukuba, Japan	Apr. 2010 – Mar. 2011
Hiroshi Takahashi	Tokyo Institute of Technology, Japan	Apr. 2010 – Mar. 2011
Yoji Kunihashi	Tohoku University, Japan	Apr. 2010 – Mar. 2011
Takumi Inaba	Tokyo University of Science, Japan	Apr. 2010 – Mar. 2011
Tatsuya Baba	Tokyo University of Science, Japan	May. 2010 – Mar. 2011
Yuta Toga	Tohoku University, Japan	Aug. 2010 – Sep. 2010
Soichiro Suzuki	Hirosaki University, Japan	Aug. 2010 – Sep. 2010
Takumi Kato	Tohoku University, Japan	Aug. 2010 – Sep. 2010
Masaya Mitsuhashi	Nagaoka University of Technology, Japan	Oct. 2010 – Feb. 2011
Takashi Aiba	Nagaoka University of Technology, Japan	Oct. 2010 – Feb. 2011
Mitsugu Kiryu	Nagaoka University of Technology, Japan	Oct. 2010 – Feb. 2011
Yuji Ueda	Waseda University, Japan	Oct. 2010 – Dec. 2010
Yusuke Takei	Tokyo University of Science, Japan	Oct. 2010 – Mar. 2011

I . Research Topics

Overview of Research in Laboratories

Materials Science Laboratory

Toshiki Makimoto

The Materials Science Laboratory aims at producing new functional materials and designing of advanced device based on novel materials and biological function. Controlling the configuration and coupling of atoms and molecules is our approach to accomplish these goals.

We have three research groups covering from thin film materials, such as nitride semiconductors, diamond, graphene, and superconductors, to biological molecules, such as receptor proteins and lipid bilayers. The distinctive characteristic of our laboratory is its effective sharing of the unique nanofabrication and measurement techniques of each group. This enables fusion of research fields and techniques, which leads to innovative material research for the future information technology.

In this year, the significant progresses have been made in the researches on the optical characteristics of AlN, the transport characteristics of graphene, and the structural observation of a receptor protein molecule.

Physical Science Laboratory

Hiroshi Yamaguchi

We are studying semiconductor and superconductor-based solid-state devices, which will have a revolutionary impact on communication and information technologies in the 21st century. In particular, we promote research of nanoscale devices fabricated using high-quality crystal growth and fine lithographic techniques.

The five groups in our laboratory are working in the following areas: precise and dynamical control of single electrons, nanodevices operating with ultra low power consumption, novel nanomechanical systems utilizing mechanical degrees of freedom in solid-state architectures, coherent quantum control of semiconductor and superconductor systems, carrier interactions in semiconductor hetero- and nanostructures, spintronics manipulating both electron and nuclear spins. We also promote the studies of cutting-edge nanolithography techniques, high-quality crystal growth, and theoretical studies including first-principle calculations.

Optical Science Laboratory

Yasuhiro Tokura

This laboratory aims for the development of core-technologies that will innovate on optical communications and optical signal processing, and seeks fundamental scientific progresses.

The groups in our laboratory are working for the quantum state control by very weak light, the search for intriguing phenomena using very intensive and short pulse light, and very small optical integrated circuits using two-dimensional photonic crystals, based on the optical properties of semiconductor nanostructures like a quantum dot.

In this year, we reported telecommunication-band singlet photon detection by MgB₂ nanowire, field experiments of quantum key distribution, observation of coherent phonon in carbon nanotubes, and first sub-femtojoule all-optical switch.

Robust Superconductivity in Pr₂CuO₄ Prepared by MBE

Hideki Yamamoto, Yoshiharu Krockenberger, Osamu Matsumoto*, Keitaro Yamagami, Masaya Mitsuhashi, and Michio Naito*
Materials Science Laboratory, *Tokyo Univ. of Agricul. & Technol.

Commonly, high- T_c cuprates are considered as doped-Mott insulators (charge transfer insulators). We have shown that the parent compounds of electron-doped superconductors, $T'-RE_{2-x}Ce_xCuO_4$ (RE : rare-earth ion) at $x = 0$ are not insulators but superconductors [1, 2]. A complex oxygen diffusion process lies beneath the contradiction of earlier reported and our present results. Superconducting parent compounds are a novelty in solid state physics and the physical origin of the superconducting state requires clarification. We have prepared high quality Pr₂CuO₄ thin films by MBE.

Superconductivity is induced after a specially designed two-step post-annealing process is applied. Systematic optimization of the annealing conditions resulted in Pr₂CuO₄ thin films with a T_c of 26 K ($\Delta T_c < 0.5$ K) and metallic conduction [$\rho_{RT} = 400 \mu\Omega\text{cm}$, RRR = 10] (Fig. 1). The resistivity value is lowest [$\rho(30\text{ K}) \sim 40 \mu\Omega\text{cm}$] for $T_{\text{red}} = 475 - 500^\circ\text{C}$ whereas T_c is highest ($T_c \sim 26$ K) for $T_{\text{red}} = 500^\circ\text{C}$. A strong diamagnetic signal was observed (Fig. 2) in parallel configuration with an onset at 23 K, confirming a robust superconducting response of Pr₂CuO₄. A nearly ideal oxygen sub-lattice and therefore intrinsic properties of the parent compounds are unveiled after applying an optimal post-annealing process. Our observations are supported by recent theoretical considerations where the parent compounds of T' -structure cuprates are not exclusively Mott insulators (charge-transfer insulators) [3, 4].

- [1] O. Matsumoto et al., Phys. Rev. B **79** (2009) 100508R.
- [2] H. Yamamoto et al., Solid State Commun. **151** (2011) 771.
- [3] C. Weber et al., Nature Phys. **6** (2010) 574; Phys. Rev. B **82** (2010) 125107.
- [4] H. Das and T. Saha-Dasgupta, Phys. Rev. B **79** (2009) 134522.

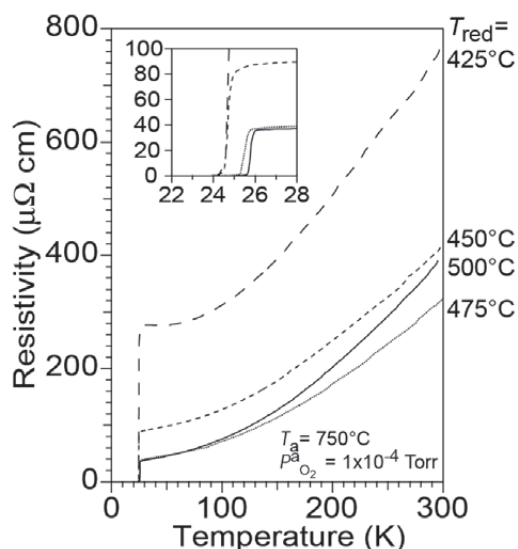


Fig. 1. Influence of the annealing temperature (T_{red}) during step II in the two-step annealing sequence on the $\rho(T)$ characteristics of the Pr₂CuO₄ films. The films were first annealed at $T_a = 750^\circ\text{C}$ and $P_{\text{O}_2}^a = 1 \times 10^{-4}$ Torr (step I).

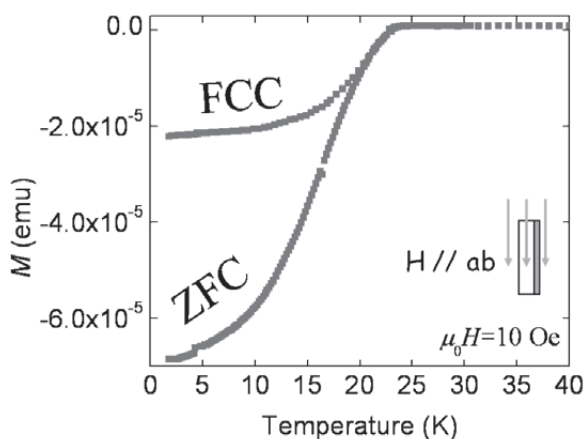


Fig. 2. Plot of Magnetization $M(T)$ curves of Pr₂CuO₄ film having the highest T_c in transport measurement. Thickness of the film is 1000 Å.

Nucleus and Spiral Growth Mechanisms of GaN Studied by Selective-Area MOVPE

Tetsuya Akasaka, Yasuyuki Kobayashi, and Makoto Kasu
Materials Science Laboratory

Crystal growth of semiconductor films generally proceeds under a combination of nucleus and spiral growth modes. In this study, we tried to clarify the mechanisms of nucleus and spiral growth modes by using selective-area metalorganic vapor phase epitaxy (MOVPE) of GaN.

First, a SiO₂ mask was deposited on a GaN (0001) bulk substrate with low density of threading dislocations. Then, the SiO₂ mask was patterned by photolithography so that it would have many hexagonal openings with the diameter of 16 μm. Finally, selective-area MOVPE of GaN films was performed on the mask-patterned GaN substrate. Source gases were ammonia and trimethylgallium. The surfaces of GaN were observed by atomic force microscopy (AFM).

A step-free GaN surface (an atomically smooth surface without any monolayer step) was formed by nucleus growth within a mask opening having no screw and mixed-type dislocations [1]. On the other hand, growth spirals were observed on a GaN surface formed within a mask opening having screw and mixed-type dislocations (Fig. 1) and the growth mode was spiral growth. The degree of supersaturation, σ , which is the driving force of crystal growth, is generally estimated from the interstep distance of a growth spiral. Figure 2 shows the nucleus and spiral growth rates plotted as a function of σ . The spiral growth rate increases parabolically with increasing σ , while the nucleus growth rate has very low values in the σ range [2]. Solid and dotted lines in Fig. 2 are fitting results we obtained using a crystal growth theory [3]. It can be seen that our experimental results are well explained by the crystal growth theory.

In summary, selective-area MOVPE enables us not only to fabricate step-free GaN surfaces but also to clarify the fundamental mechanisms of crystal growth including nucleus and spiral growth.

[1] T. Akasaka et al., *Appl. Phys. Express* **2** (2009) 191002.

[2] T. Akasaka et al., *Appl. Phys. Lett.* **97** (2010) 141902.

[3] W. K. Burton et al., *Phil. Trans. Roy. Soc. A* **243** (1951) 299.

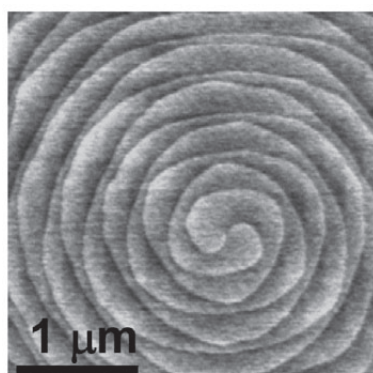


Fig. 1. AFM image of a growth spiral center of GaN.

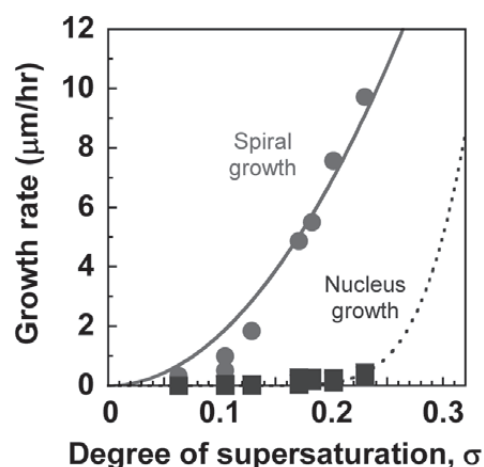


Fig. 2. Nucleus and spiral growth rates plotted as a function of the degree of supersaturation.

Emission Mechanism of AlN Deep-Ultraviolet Light-Emitting Diode

Yoshitaka Taniyasu and Makoto Kasu
Materials Science Laboratory

Aluminum nitride (AlN) is a direct-bandgap semiconductor with a bandgap energy of 6 eV, the largest among semiconductors. Therefore, AlN is a promising material for deep-ultraviolet (deep-UV) light-emitting devices with an ultrashort wavelength. Previously, we achieved both n-type and p-type doping in AlN and fabricated an AlN p-n junction light-emitting diode (LED) with near-band-edge electroluminescence (EL) at a wavelength of 210 nm, the shortest ever reported for any kind of LED [1]. Here we identify the origin of the near-band-edge emission and propose a high-efficiency LED structure based on the unique characteristic that the emission intensity largely changes depending on the crystal planes of its surface.

First, a C-plane AlN p-n junction LED structure was grown on C-plane SiC substrate by metalorganic vapor phase epitaxy. By increasing the NH₃ flow rate, the hole concentration in the p-type AlN was increased because of the suppressed formation of N vacancies, which act as compensating donors. As a result, the LED external quantum efficiency was increased from 8×10^{-6} to 1×10^{-4} % [2]. As shown in Fig. 1, the near-band-edge emission was dominated by an exciton emission originating from the crystal-field split-off valence band (FX_{CH}), but another exciton emission originating from heavy/light hole valence bands (FX_{HH/LH}) was also observed. From the emission energies, considering residual strain, the crystal-field splitting energy Δ_{CR} was determined to be -165 meV. Because of the negative Δ_{CR} , the topmost valence band is the crystal-field split off valence band with a p_z-like state and then the near-band-edge emission polarizes for the electric field parallel to the c-axis (E||c). Consequently, the near-band-edge emission is weak from the C-plane but strong from the A-plane for AlN.

For nitride semiconductors, like AlN and GaN, the C-plane is preferable for high-quality growth and therefore a C-plane LED structure has been commonly fabricated. However, for AlN, because of the E||c polarization, an A-plane LED structure is desirable for enhancing the light extraction and improving the emission efficiency. We fabricated the A-plane LED structure by using A-plane SiC substrate and observed a near-band-edge emission at 210 nm [3]. As shown in Fig. 2, the A-plane LED showed strong emission from the LED surface ($\theta_R = 0^\circ$), while the conventional C-plane LED showed weak emission. Thus, the A-plane LED is a promising structure for high-efficiency AlN deep-UV LED.

- [1] Y. Taniyasu, M. Kasu, and T. Makimoto, *Nature* **441** (2006) 325.
 [2] Y. Taniyasu and M. Kasu, *Appl. Phys. Lett.* **98** (2011) 131910.
 [3] Y. Taniyasu and M. Kasu, *Appl. Phys. Lett.* **96** (2010) 221110.

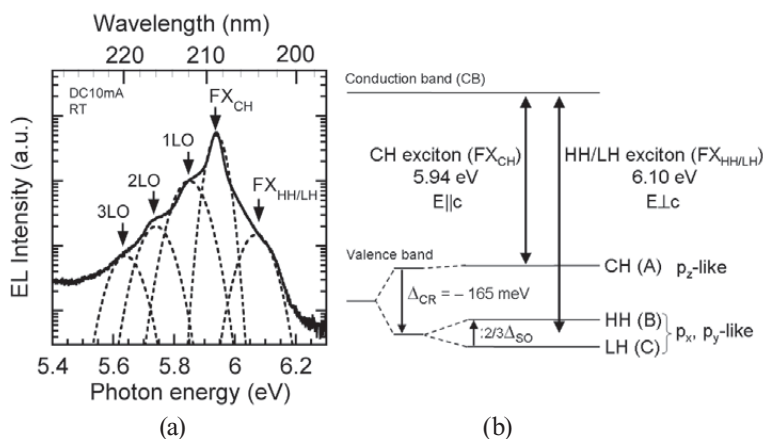


Fig. 1. (a) Emission spectrum of AlN LED and (b) optical transitions in AlN.

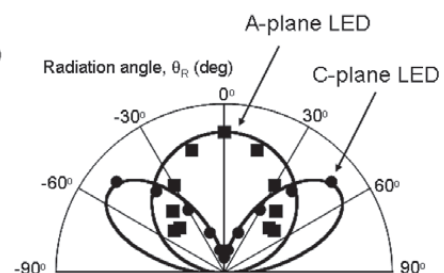


Fig. 2. Radiation patterns of A-plane and C-plane AlN LEDs.

AlGaN/GaN HEMTs Epitaxially Grown on Single-Crystal Diamond

Kazuyuki Hirama, Yoshitaka Taniyasu, and Makoto Kasu
Materials Science Laboratory

AlGaN/GaN high-electron mobility transistors (HEMTs) are being developed extensively for RF high-power applications. However, the output power of AlGaN/GaN HEMTs is limited by the thermal conductivities of the substrate materials. Among all materials, single-crystal diamond has the highest thermal conductivity of ~ 22 W/cmK. Therefore, diamond is expected to be the ideal substrate for high-power devices. However, due to the difference in the crystal structures of nitride semiconductors and diamond, single-crystal nitride growth on diamond substrates is difficult. Recently, using (111) surface orientation, we have successfully grown single-crystal AlN (0001) layers on diamond substrates [1, 2].

Here, using the single-crystal AlN as a buffer layer, we epitaxially grew the AlGaN/GaN HEMT structure on diamond (111) substrate. As shown in Fig. 1, first, a 180-nm-thick AlN buffer layer was grown, followed by the growth of 20-period AlN(3 nm)/GaN(17 nm) multi layers, a 600-nm-thick GaN layer, a 1-nm-thick AlN spacer layer, a 30-nm-thick $\text{Al}_{0.25}\text{Ga}_{0.75}\text{N}$ barrier layer, and a 4-nm-thick GaN cap layer. From X-ray diffraction measurements, we confirmed the single-crystal growth of the AlGaN/GaN HEMT structure. Next, we confirmed the formation of two-dimensional electron gas (2DEG) in the AlGaN/GaN heterostructure by Hall-effect measurement. The sheet electron density at room temperature was $1 \times 10^{13} \text{ cm}^{-2}$. On the other hand, the electron mobility at room temperature was $730 \text{ cm}^2/\text{Vs}$.

A 3- μm -gate-length AlGaN/GaN HEMT on the diamond substrate showed the maximum I_{DS} of 220 mA/mm. Figure 1 shows the high-frequency small-signal characteristics. From the frequency dependence of the current gain ($|H_{21}|^2$), maximum stable gain (MSG) and maximum power gain (MAG), the cut-off frequency (f_T) of 3 GHz and maximum frequency of oscillation (f_{max}) of 7 GHz were obtained. Then, we compared the device temperature of AlGaN/GaN HEMTs on diamond and SiC substrates under high-DC-power operation. Figure 2(a) shows the setup for measuring the device temperatures. Figures 2(b) and (c) show the temperature distributions from the side of the AlGaN/GaN HEMTs on the diamond and SiC substrates at a dissipated power of 2 W (3.2 W/mm). The device temperature at 2 W increased from 23 to 36°C (temperature rise $\Delta T = 13^\circ\text{C}$). On the other hand, on the SiC substrate, the device temperature increased from 23 to 46°C ($\Delta T = 23^\circ\text{C}$). From the dissipated power dependence of the device temperature rise [Fig. 2(d)], we estimated the thermal resistance of the AlGaN/GaN HEMT on the diamond substrate to be 4.1 Kmm/W, which is about half of that on a SiC substrate (7.4 Kmm/W) [3]. The low thermal resistance for the AlGaN/GaN HEMT on the diamond substrate is attributed to the high thermal conductivity of the single-crystal diamond. These results show that AlGaN/GaN HEMTs on diamond are promising for high-frequency and high-power applications.

[1] Y. Taniyasu and M. Kasu, *J. Cryst. Growth* **311** (2009) 2825.

[2] K. Hirama, Y. Taniyasu, and M. Kasu, *J. Appl. Phys.* **108** (2010) 013528.

[3] K. Hirama, Y. Taniyasu, and M. Kasu, *Appl. Phys. Lett.* **98** (2011) 162112.

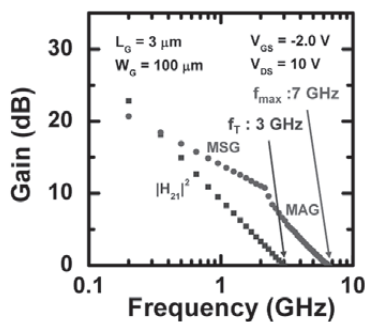


Fig. 1. High-frequency small-signal characteristics of AlGaN/GaN HEMT on diamond (111).

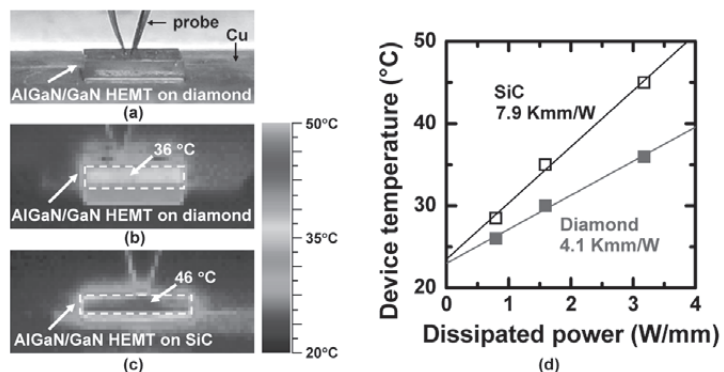


Fig. 2. (a) Setup for measuring the temperature distributions. Temperature distribution of the AlGaN/GaN HEMTs on (b) diamond and (c) SiC substrates at a dissipated power of 2 W (3.2 W/mm). (d) Dissipated-power dependence of device temperature for AlGaN/GaN HEMTs on the diamond and SiC substrates. Closed and open squares indicate the temperatures for diamond and SiC substrates, respectively.

Highly Integrative Artificial Cell Membrane Microarray

Kazuaki Furukawa
Materials Science Laboratory

Microarrays of biological molecules such as DNA chips are widely used for high-throughput bioanalysis. When developing new microarrays, it is essential to improve the technology for fixing biomolecules without losing their biological functionality. A microarray consisting of an artificial cell membrane supported on a solid surface is expected to provide an important platform for the purpose. We have developed a new technique for fabricating an artificial cell membrane microarray and demonstrated a biosensing application of the fabricated microarray.

We used the self-spreading phenomenon, which is a self-organizing process that forms a cell membrane at a solid-liquid interface, to fabricate the artificial cell membrane microarray. Our method is unique in that the position of the self-spreading is controlled with a hydrophilic/hydrophobic pattern [1]. According to the designed pattern, a self-spreading membrane starting from a macroscopic area was guided to the microarray structure without mixing with membranes in the different areas. We succeeded in fabricating 10- μm -width parallel lines, each filled with an artificial cell membrane with a unique composition, at 5- μm intervals (color frontispiece). Structures obtained with our new technique are in principle more than 100 times more highly integrated than previously reported structures that employ the vesicle fusion technique on patterned surfaces [2].

To demonstrate the validity of the microarray for biosensing applications, we fabricated a composition microarray, part of which contained biotin-conjugated lipid. Figure 1 shows fluorescence images of the array that were recorded (a) before and (b) after it was immersed in Texas Red conjugated streptavidin solution. Red fluorescence, which originates from Texas Red, was observed only in the lines containing biotin-conjugated lipids after 90 min, as shown in Fig. 1(b). This is due to the specific binding between biotin and streptavidin. Since the red fluorescence from the lines without biotin is limited, the microarray is valuable for biosensing applications.

This work was supported by KAKENHI.

- [1] K. Furukawa et al., *Lab Chip* **6** (2006) 1001.
[2] K. Furukawa and T. Aiba, *Langmuir* **27** (2011) 7341.

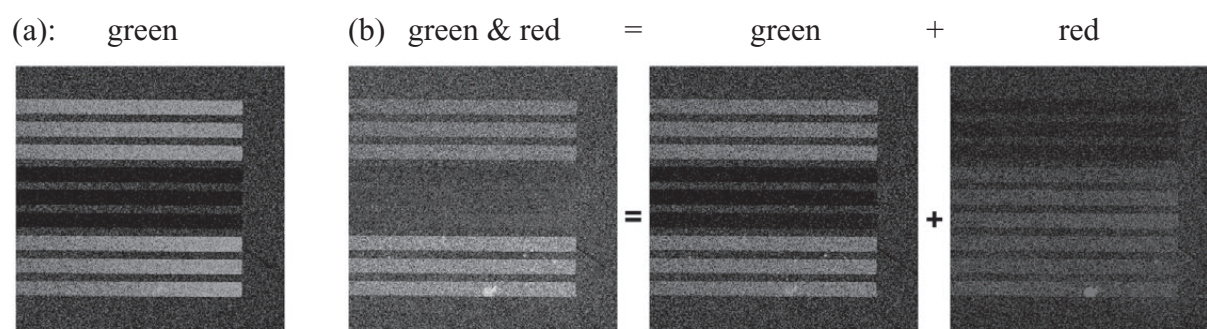


Fig. 1. Fluorescence images of artificial cell membrane microarray (a) before and (b) 90 min after the addition of Texas Red conjugated streptavidin solution. The membranes are composed mainly of Egg-PC with top 3 lines: 1 mol% NBD-conjugated lipid; middle 3: 1 mol% biotin-conjugated lipid; bottom 3: both lipids. The green and red fluorescence is from NBD and Texas Red, respectively, and the green & red image in (b) is a superimposition of two images, green and red.

Evaluation of Carrier Density in Doped Single-Wall Carbon Nanotubes

Satoru Suzuki and Hiroki Hibino
Materials Science Laboratory

The thermal chemical vapor deposition (CVD) method has been widely used to grow single-wall carbon nanotubes (SWNTs). However, direct growth of doped SWNTs and tuning of the impurity concentration in them are still a big challenge. Another very important issue for doped SWNTs is their characterization. In particular, it is very difficult to evaluate carrier concentrations in individual SWNTs. Thus, the carrier concentration has not been clarified in previous studies of doped SWNTs. In this study, we grew boron (B)- and nitrogen (N)-doped SWNTs from B- and N-containing feedstocks by the thermal CVD method. Raman spectral shifts induced by carrier doping were clearly observed and the carrier densities were evaluated from the shifts [1].

We used triisopropylborate ($C_9H_{21}BO_3$) and benzylamine (C_7H_9N) as B- and N-containing feedstocks. These chemicals also acted as a carbon source, and we did not use any other carbon sources. B- or N-doped SWNTs were grown from either one or the other feedstock, with a Co thin film deposited on a SiO_2/Si substrate used as a catalyst. We were also able to synthesize BN-doped SWNTs by supplying both triisopropylborate and benzylamine simultaneously, as shown in Fig. 1. Transmission electron microscopy and Raman (radial breathing mode) measurements indicated that the diameter of the doped SWNTs is mostly 1–2 nm, like that of undoped SWNTs grown using a similar catalyst. Figure 2 shows Raman (G band) spectra of B-, N-, and BN-doped SWNTs, and undoped SWNTs. As can be seen in the figure, the G band position in the doped SWNTs is shifted to the high-wavenumber side by $3\text{--}6\text{ cm}^{-1}$, regardless of the choice of feedstock. The hardening of the G band regardless of doping type (electron or hole doping) can be understood as renormalization of phonon energy through electron-phonon coupling induced by a Fermi level shift in a semiconducting SWNT. Originally, the energy of the G band phonon is softened by the electron-phonon interaction (Kohn anomaly). However, a Fermi level shift reduces the electron-phonon interaction and thus, reduces the effect of the Kohn anomaly. Consequently, the Fermi level shift induced by electron or hole doping causes a hardening of the G band. The G band hardening is expected to become prominent when the Fermi level reaches the valence or conduction band. Therefore, the results shown in Fig. 2 indicate that the Fermi level in the doped SWNTs is located inside the valence or conduction band. We can also estimate the carrier density. Assuming that the SWNT diameter is 1.5 nm, the estimated carrier concentration reaches 0.4–0.8%, which is a considerably large value.

[1] S. Suzuki and H. Hibino, *Carbon* **49** (2011) 2264.

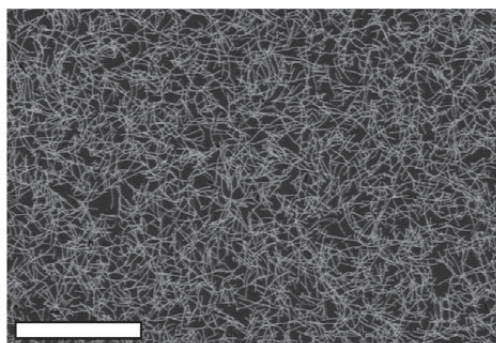


Fig. 1. SEM image of BN-doped SWNTs. Scale bar: 5 μm .

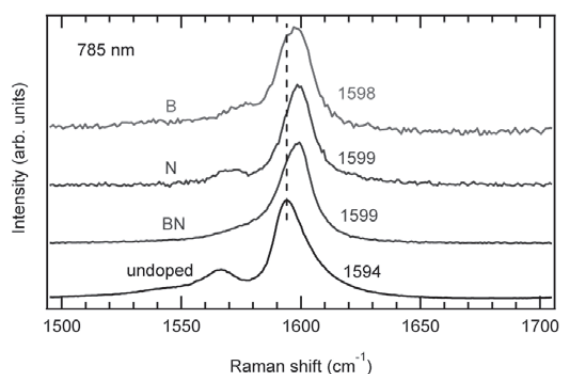


Fig. 2. G band spectra of B-, N-, and BN-doped SWNTs. The peak positions are denoted. The excitation wave length was 785 nm.

Transport Properties of Epitaxial Monolayer and Bilayer Graphene

Shinichi Tanabe¹, Yoshiaki Sekine², Hiroyuki Kageshima², Masao Nagase³, and Hiroki Hibino¹
¹Materials Science Laboratory, ²Physical Science Laboratory, ³The University of Tokushima

Monolayer and bilayer graphene have gained significant attention because of their potential applications for high-frequency devices and for logic devices, respectively. The mechanical exfoliation of graphite is a common way of making graphene because high-quality graphene can be obtained. However, this technique is only good for making graphene flakes of only a few tens micrometers in size. For wafer-scale synthesis of graphene, we employ thermal decomposition of SiC, which enables epitaxial growth of graphene layers. By annealing SiC(0001) in an Ar atmosphere and in an UHV environment, we have succeeded in growing monolayer and bilayer graphene, respectively. To elucidate the transport properties of these graphene, we systematically studied the electrical properties of monolayer and bilayer graphene in top-gate devices.

Figure 1 shows the magnetic-field dependences of longitudinal resistance and Hall resistance of the monolayer-graphene device. The magnetic field was applied perpendicular to the graphene plane. The Hall resistances become constant as a function of magnetic field at the resistances unique to monolayer graphene, where, at the same time, the longitudinal resistances show minima. At high-magnetic field, the minimum resistance of the longitudinal resistance becomes zero, which is a hallmark of the quantum Hall state. By decreasing the carrier density with applying gate voltage (V_g), the mobility increases, and the mobility at 2 K exceeded $10,000 \text{ cm}^2 \text{ V}^{-1} \text{ s}^{-1}$ at a carrier density of $3 \times 10^{10} \text{ cm}^{-2}$, which is comparable to that of exfoliated graphene transferred onto SiO_2 [1]. Figure 2 shows the gate-voltage dependence of resistance of the bilayer-graphene device from 2 to 300 K. In all temperatures, resistance at the charge neutrality point (CNP) shows maximum resistance [2]. The strong temperature dependence of the resistance at the CNP results from band gap opening due to the interaction of the graphene with the substrate. The observed quantum Hall effect in the monolayer-graphene device proves high quality of the monolayer graphene and the electrical detection of the band gap in bilayer-graphene device is an important finding for its applications. These results show that the thermal decomposition of SiC is an effective method to grow monolayer and bilayer graphene.

This work was supported by KAKENHI.

[1] S. Tanabe et al., *Appl. Phys. Express* **3** (2010) 075102.

[2] S. Tanabe et al., *Jpn. J. Appl. Phys.* **50** (2011) 04DN04.

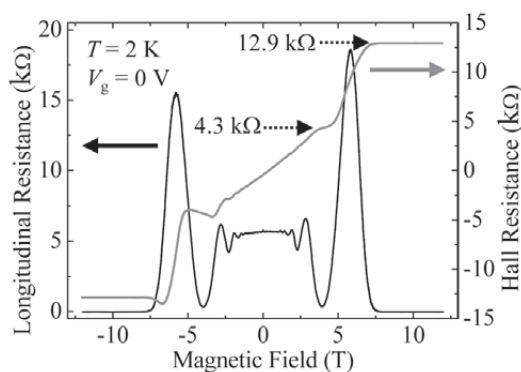


Fig. 1. Temperature dependence of longitudinal resistance and Hall resistance of monolayer graphene.

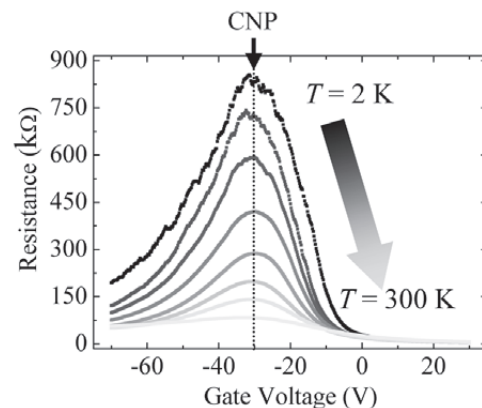


Fig. 2. Gate-voltage dependence of resistance of bilayer graphene from 2 to 300 K.

Manipulation of Biomolecules on Solid Substrate Using Artificial Cell Membrane

Hiroshi Nakashima and Kazuaki Furukawa
Materials Science Laboratory

The development of biofunctional devices requires a biointerface for maintaining biomolecules on a substrate without interfering with their structure or biological functions. By using an artificial membrane biointerface, we can control the position, density and arrangement of biomolecules, leading to the design of various bio devices such as highly sensitive biosensors or implant-type biochips. Here we produced artificial cell membranes on a substrate that enable proteins to be adsorbed or transported to a desired position, and thus realized a novel molecular manipulation technique for use at the biointerfaces [1].

A cell membrane is essentially composed of phospholipids (lipids). The fluidity of an artificial cell membrane is controlled by the choice of lipid components. We selectively fabricated artificial cell membranes with high/low fluidity that contained nickel-chelating lipids (Ni-lipid). The Ni-lipid is capable of specific binding with terminal modified proteins. Figure 1(a) and (b) shows AFM images of an artificial cell membrane consisting of DSPC (low fluid lipid) and Ni-lipid. The image of a 50/50 mol% of DSPC/Ni-lipid reveals a heterogeneous membrane structure with round DSPC-rich domains distributed in a Ni-lipid-rich fluid-phase domain. The DSPC domains were slightly thicker (1.0 nm) than the surrounding Ni-lipid domain. The area of each domain was controlled by controlling the molar ratio of the lipid components. When histidine-tagged green fluorescent proteins (His-tagged GFPs) were added to the membrane, the fluorescent pattern was evidently based on the specific adsorption of His-GFPs only in the Ni-lipid domain [Fig. 1 (c) and (d)]. While the membrane produced by DOPC (high fluid lipid) and Ni-lipid formed a homogeneous structure with high fluidity. The membrane exhibited a self-spreading ability in buffer solution whereby a single lipid membrane (5 nm high) grows on a substrate surface by self-organization [2]. By employing the self-spreading nature, we demonstrated protein transport along the micro-pattern. Figure 2 shows the time evolution of the molecular transport of His-GFPs tethered on the membrane. The transport property agreed well with the existing self-spreading model of an artificial membrane [velocity (v) = ($\beta/\text{time } (t)$)^{1/2}] where the kinetic spreading coefficient (β) was 10.4 $\mu\text{m}^2/\text{s}$.

The biointerface produced by lipids can also employ a cell membrane model to analyze biomolecular interactions or signal transmission events. Therefore, the biointerface will be beneficial for bioscience as well as providing a framework for building biofunctional devices.

[1] H. Nakashima et al., *Langmuir* **26** (2010) 12716.

[2] K. Furukawa et al., *Lab Chip* **6** (2006) 1001.

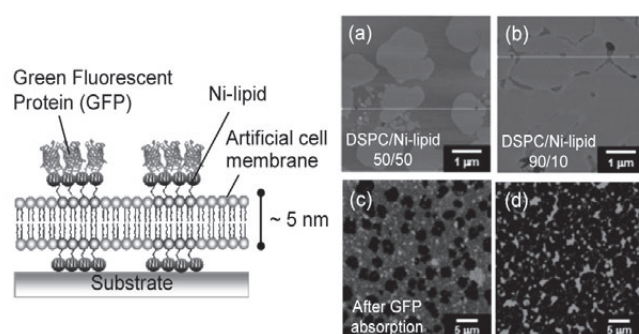


Fig. 1. Pattern formation of artificial cell membrane and absorption of proteins at specific location on membrane.

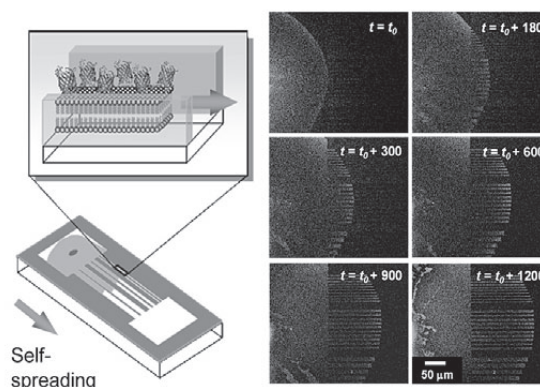


Fig. 2. Protein transport through self-spreading of artificial cell membrane.

AFM Observation of a Receptor Subunit Structure

Nahoko Kasai, Aya Tanaka, and Chandra S. Ramanujan*
Materials Science Laboratory, *University of Oxford

Membrane receptor proteins play the crucial role of transmitting signals in the central nervous system. They are regulated by chemicals called ligands which bind to the extracellular ligand binding domains. This binding either effects a change in the protein that forms a pore allowing movement of charged ions into the cell or modifies inside the cells chemically. As such, receptor proteins are small but highly selective devices. Most of the receptor proteins consist of multiple subunit proteins. The structure of the receptor proteins has been examined by mainly by X-ray crystallography and cryo-EM, however, these techniques do not allow the examination of functioning receptors. Atomic force microscopy (AFM) enables the nano-scale observation of proteins in a liquid environment, offering a unique opportunity to observe functional biological molecule such as single proteins under physiological conditions.

We have succeeded in observing the structure of single purified and ionotropic receptor proteins in the solution using the AFM [1]. In this study, receptor proteins were purified from over-expressed insect cells (Fig. 1), and then reconstituted into an artificial lipid bilayer by dialysis because the receptors would function as *in vivo* when reconstituted into the lipid bilayer. Receptor samples were settled on to mica substrate and rinsed thoroughly. We then imaged the reconstituted receptor proteins on a substrate in a buffer solution using AFM. We determined the orientation of the reconstituted receptor using antibody reaction, and then we magnified and found four protrusions indicating tetrameric structure of the protein (Fig. 2), which provides various different shapes of the single receptor. This result first demonstrated that the structure of the functioning receptor proteins seems to change mainly by heat fluctuation.

This research was supported in part by Bio-nanotechnology IRC in UK and by KAKENHI .

[1] N. Kasai et al., BBA Gen. Subj. **1800** (2010) 655.

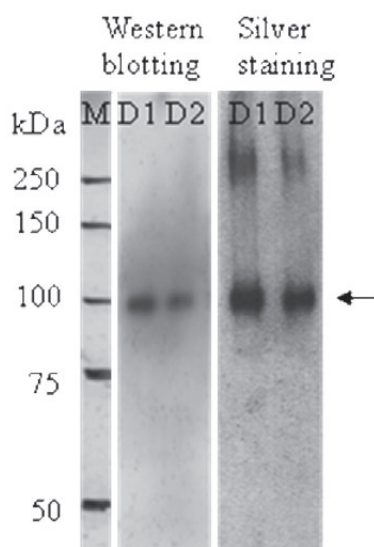


Fig. 1. Electrophoresis analysis of purified ion-channel receptor protein.

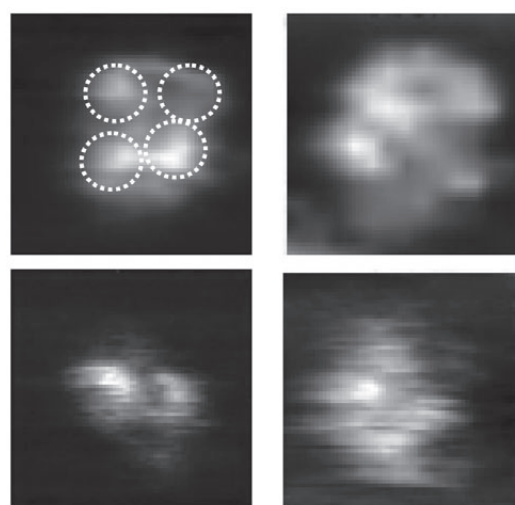


Fig. 2. AFM images of subunit structured ion-channel receptor protein reconstituted into artificial lipid bilayer. (100x100 nm)

Electrostatic Control of Artificial Cell Membrane Self-Spreading

Yoshiaki Kashimura and Kazuaki Furukawa
Materials Science Laboratory

A lipid bilayer, which is a fundamental component of a cell membrane, can be spread artificially on a substrate by self-assembly. Using this self-spreading nature of an artificial cell membrane (ACM), we have investigated the effect of a single nanogap structure on the molecular dynamics within an ACM [1, 2]. We report here the electrostatic control of ACM self-spreading by the temporal switching of an electric field applied to a nanogap structure [3].

A pair of electrodes with a nanogap was fabricated using Au/Ti. A 10 μm wide microchannel with wells at both ends was fabricated on this nanogap structure. A lipid mixture consisting of Egg-PC and Egg-PG (molar ratio 7:3) containing 1 mol% Texas Red-DHPE was attached to one of the wells. The self-spreading of an ACM was initiated by immersing the substrate in a buffer solution containing 0.1–100 mM NaCl.

Figure 1 shows a typical time evolution for a self-spreading ACM induced by the temporal switching of the applied voltage when we used a 100 mM NaCl solution and a nanogap with a separation of <5 nm. Before the ACM passed through the nanogap, no voltage-dependent changes in the self-spreading were observed [Fig. 1(a) and (b)]. However, when the ACM reached the nanogap, the self-spreading was forcibly prevented by the voltage application [Fig. 1(c)]. This continued for ~ 300 s, corresponding to the interval of the voltage application [Fig. 1(d)]. Interestingly, the ACM started to develop again immediately after the applied voltage was returned to 0 V [Fig. 1(e)-(g)]. Furthermore, we confirmed that this ON/OFF switching of the self-spreading behavior could be repeatedly observed, corresponding to the temporal switching of the applied voltage [Fig. 1(h)-(l)]. The electric double layer, which is characterized by the Debye length, plays a crucial role in this behavior. In a bulk condition, the electric field is shielded by counterions in the electrolyte solution. In contrast, the sum of the Debye length (D) from both electrode surfaces (a few nanometers for a 100 mM NaCl solution) is close to the nanogap width (d), the electric field can be effectively applied in the nanogap spacing, leading to the electrostatic trapping of lipid molecules. A continuous supply of lipid molecules is vital for the self-spreading. Therefore, the electric field applied to a nanogap acted as a molecule gate for the self-spreading (Fig. 2). The technique described here constitutes the first demonstration of the temporal and spatial control of biomembrane development in a nanometer-scale device and can provide new opportunities for the realization of nanobio devices.

This work was supported by KAKENHI.

- [1] Y. Kashimura et al., Jpn. J. Appl. Phys. **47** (2008) 3248.
- [2] Y. Kashimura et al., Jpn. J. Appl. Phys. **49** (2010) 04DL15.
- [3] Y. Kashimura et al., J. Am. Chem. Soc. **133** (2011) 6118.

Fig. 1. (right). Time evolution of a self-spreading ACM.

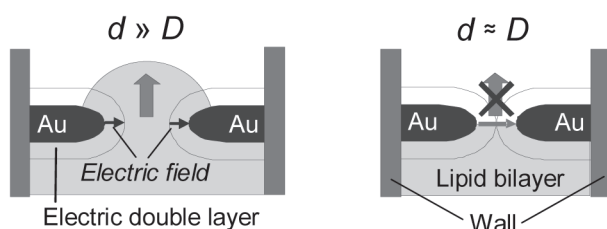
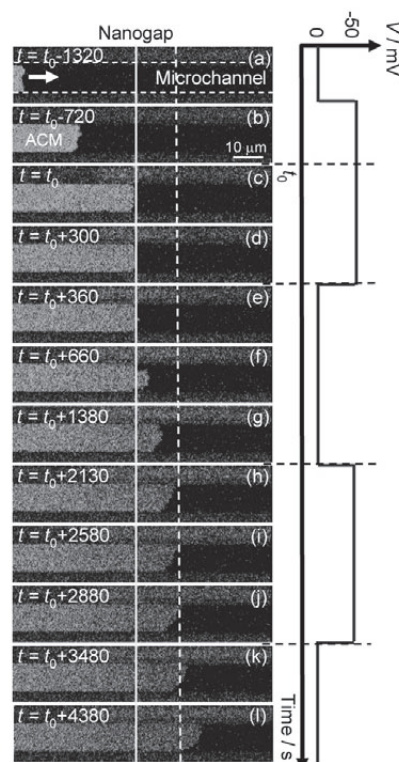


Fig. 2. (upper). Mechanism of electrostatic trapping.



Single-Electron Resonant Activation over an Oscillating Barrier

Satoru Miyamoto^{1,2}, Katsuhiko Nishiguchi¹, Yukinori Ono¹,
Kohei M. Itoh², and Akira Fujiwara¹
¹Physical Science Laboratory, ²Keio University

Single-electron (SE) transfer device has been investigated from the viewpoints of its application to metrological current standards and low power circuits. At relatively high temperatures the device is also a good platform to study the dynamics of Brownian particles. In this work we address resonant activation of a particle over an oscillating barrier [1], which is known as one of the resonant phenomena for classical particles. Such resonance is predicted to occur when the oscillation frequency satisfies the condition of scale matching with the average rate of the particles crossing the barrier. Until now only the resonant activation of macroscopic variables has been observed in tunnel diodes and Josephson junctions.

The measured device consists of a silicon nanowire with multiple finger gates as shown in Fig. 1 (a). Figure 1 (b) describes how the SE transfer is performed using a SE ratchet [2] scheme, which enables clocked transfer of SEs from source to drain via a charge island. Using proper gate voltages, we can create a situation where a SE in the island is thermally activated over a potential barrier as shown in Fig. 1(c). Then we apply a small *rf* signal A_{rf} with a frequency f_{rf} to introduce a modulation U_m to the barrier. The SE transfer is performed at 16 K with the ratchet clock frequency of $f_{RC}=16.6$ MHz. The average escape time τ_{avg} is evaluated by measuring the transfer current by varying the ejection time t_{G1L} during which the electron is thermally activated over the barrier. Figure 2 shows τ_{avg} as a function of f_{rf} at different gate voltages V_{G1L} which are used to change the order of τ_{avg} . τ_{avg} is found to manifest a resonance at a frequency with the same order of $1/\tau_{avg}$. Furthermore, the resonant frequency f_{RES} exhibits a shift to higher frequencies for a shorter τ_{avg} . These behaviors are well explained in the framework of the resonant activation which happens due to the synchronization between the deterministic *rf* signal and the stochastic escape of a single electron as a Brownian particle [3].

- [1] C. R. Doering and J. C. Gadoua, Phys. Rev. Lett. **69** (1992) 2318.
[2] A. Fujiwara, K. Nishiguchi, and Y. Ono, Appl. Phys. Lett. **92** (2008) 042102.
[3] S. Miyamoto et al., Phys. Rev. B **82** (2010) 033303.

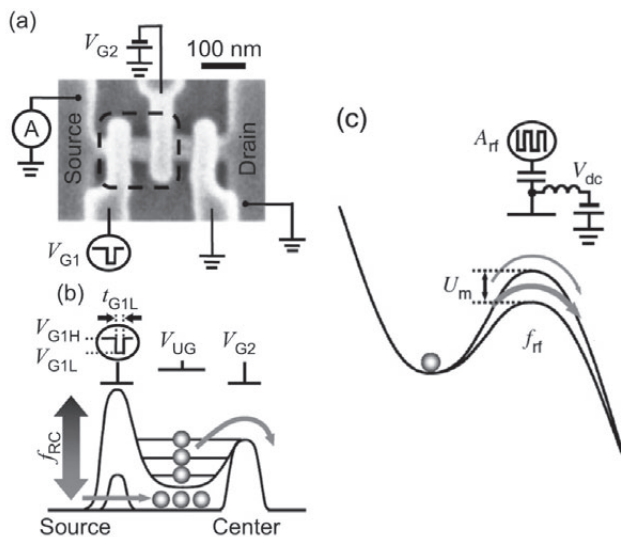


Fig. 1. (a) Top-view scanning electron micrograph and (b) schematic potential diagram of the single-electron ratchet. (c) Single-electron escape over an oscillating barrier.

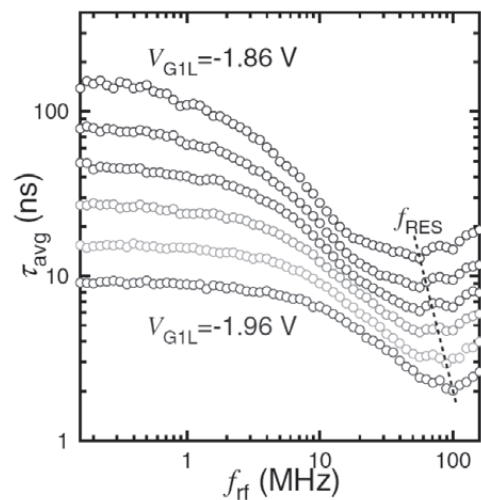


Fig. 2. *rf*-frequency dependence of the average escape time at different values of V_{G1L} which give different barrier heights.

Theoretical Study of Magnetoelectric and Thermoelectric Properties of Graphene

Hiroyuki Kageshima¹, Hiroki Hibino², Masao Nagase³,
Yoshiaki Sekine¹, and Hiroshi Yamaguchi¹

¹Physical Science Laboratory, ²Materials Science Laboratory, ³The University of Tokushima

Graphene is atomically thin two-dimensional sheet. Because of this unique structure, it is expected to show various novel properties. We theoretically study its potential [1-3].

Magnetoelectric effect controls magnetism by external electric field [1, 3]. Graphene edge with the zigzag structure is theoretically predicted to show magnetism. However, the magnetism is difficult to be realized if the graphene is located on SiO₂ substrate, because the edge should be appropriately terminated by H atoms. On the other hand, in case of epitaxial graphene on SiC(0001) substrate, experiments show that islands of graphene are already formed in the initial stage of the growth by the high-temperature annealing. In addition, it is theoretically revealed that the island edge is already connected seamlessly to the SiC substrate (Fig. 1). Therefore, the edge is not necessary to be terminated by H atoms. Since the epitaxial graphene is also negatively charged due to the interaction with the substrate, and since the edge magnetism requires the charge neutrality, the island with the zigzag structure edge shows magnetism, only when the application of external field by a gate electrode induces positive charge to neutralize the epitaxial graphene. In this way, the magnetism appears by the magnetoelectric effect for the graphene islands on SiC (Fig. 1).

Thermoelectric effect induces the potential difference from the temperature difference. It is useful for the electric power generation from wasted heat [2, 3]. The conventional graphene on SiO₂ substrate shows the thermoelectric figure of merit ZT_0 of the order of 10^{-3} , which means high difficulty for the practical use. However, if the density of ionic adsorbates on graphene is reduced by 1/1000 times and the optical phonon scattering from the substrate is suppressed significantly, the graphene is expected to exhibit the figure of merit ZT_0 over 1 around the charge neutrality point, which means the strong possibility for the practical use (Fig. 2). Graphene is plentiful, cheap, harmless, and low in specific gravity. Therefore, graphene is a good candidate for a practical thermoelectric conversion material.

This work is partly supported by KAKENHI.

[1] H. Kageshima et al., Appl. Phys. Express **3** (2010) 115103.

[2] H. Kageshima, Jpn. J. Appl. Phys. **49** (2010) 100207.

[3] H. Kageshima et al., Jpn. J. Appl. Phys., in press.

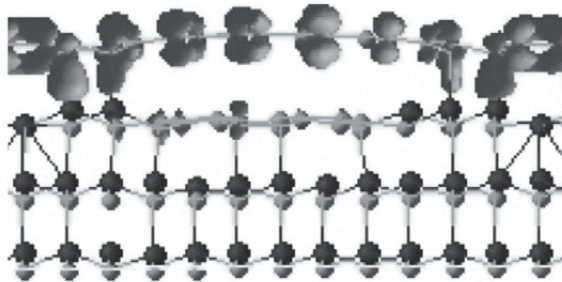


Fig. 1. Atomic structure of graphene with zigzag edges on SiC(0001) and the spin polarization distribution when the induced charge is $+8e$. Large and small circles are Si and C atoms, respectively.

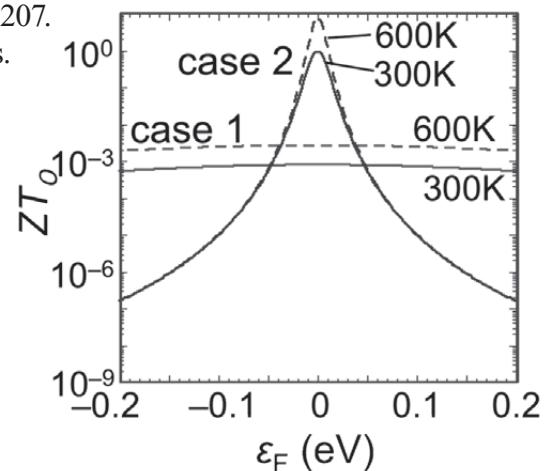


Fig. 2. Thermoelectric figure of merit ZT_0 of graphene as the function of the Fermi energy position ϵ_F . Conventional case (case 1) and suppressed carrier scattering case (case 2).

Strong Stark Effect in Electroluminescence from Phosphorous-Doped SOI-MOSFETs

Jin-ichiro Noborisaka, Katsuhiko Nishiguchi, Yukinori Ono,
Hiroyuki Kageshima, and Akira Fujiwara
Physical Science Laboratory

The electronic states of phosphorous atoms in silicon (Si) are now attracting much attention because they could be useful for solid-state quantum computers. We report a strong Stark effect in electroluminescence (EL) from phosphorous-doped silicon-on-insulator (SOI)-MOSFETs when electrons are injected into the sub-10-nm-thick SOI channel by tunneling [1].

The devices were SOI-MOSFETs with an n-type polycrystalline Si (poly-Si) tunneling gate [Fig. 1(a)]. Two SOI thicknesses (t_{SOI}) of 8.5 and 25 nm were prepared. The thicknesses of the front-gate oxide (FOX), and the buried oxide (BOX) were approximately 2 and 400 nm, respectively. The potential profiles for the device are shown in Fig. 1(b). Due to the thermal treatment for the device fabrication, the SOI channel was phosphorous-doped on the order of 10^{17} cm^{-3} . Electroluminescence spectra were taken at temperature (T) of 80 K. Electrons are injected from the front gate into the SOI channel, while holes are injected from the boron doped p^+ contact. Figure 2(a) shows the V_{BG} dependence of the EL spectrum for the device with t_{SOI} of 25 nm. The EL intensity decreased as V_{BG} was positively increased, producing an electric field in the SOI so that electrons distribute near BOX/SOI interface. Then electrons and holes are strongly separated, which results in the decrease of the EL intensity. On the other hand, the V_{BG} dependence of the EL spectra for t_{SOI} of 8.5 nm showed complicated behavior [Fig. 2(b)]. The peak for a neutralized donor and free-hole recombination ($D^0\text{-h}$) showed Stark shift of up to 50 meV at V_{BG} of 136 V. The EL intensity kept a higher value even when that for 25 nm became almost zero, and then suddenly decreased around V_{BG} of 80 V [Fig. 2(c)]. The sudden change of the EL intensity can be explained by electron dissociation from strongly bound states. In contrast to the thicker QW, the ground state of triangular well at the BOX interface in the QW for t_{SOI} of 8.5 nm is higher than that of phosphorous-bound state at low electric field. Therefore, electrons bound at phosphorous atoms hardly dissociate in the thin QW. This is the reason for the difference in the specific field needed to cause the sudden decrease of the EL intensity.

[1] J. Noborisaka et al., Appl. Phys. Lett. **98** (2011) 033503.

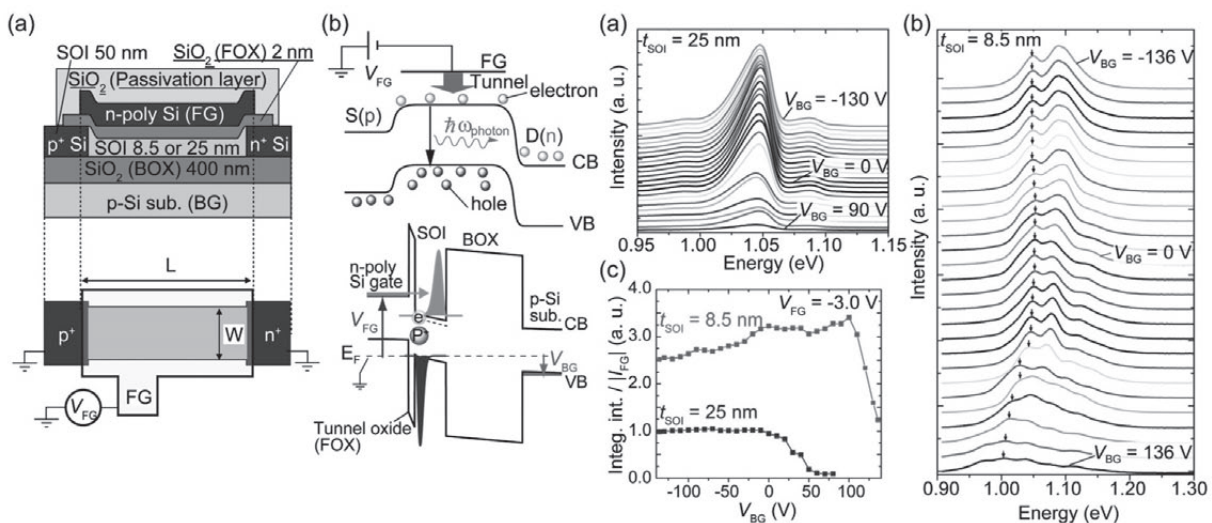


Fig. 1. (a) Schematic cross section of the device structure (top) and top view of the device (bottom). (b) Potential profile from source to drain (top) and from top to bottom of the device (bottom).

Fig. 2. (a) The V_{BG} dependence of EL for $t_{\text{SOI}} = 25 \text{ nm}$. (b) That for $t_{\text{SOI}} = 8.5 \text{ nm}$. The arrows trace the peak for $D^0\text{-h}$. The voltage steps for V_{BG} are 10 V except for $|V_{\text{BG}}|$ of 136 V. (c) The V_{BG} dependence of the integrated EL intensity.

Parametric Frequency Conversion and Logic Operations Using Electromechanical Resonators

Imran Mahboob, Emmanuel Flurin, Katsuhiko Nishiguchi,
Akira Fujiwara, and Hiroshi Yamaguchi
Physical Science Laboratory

The pioneering mechanical computer has been largely forgotten with the advent of Boolean logic, the semiconductor transistor and integrated circuits which have given rise to logic gates that underpin all modern computation [1]. However as conventional computers toil to conserve Moore's law, the nanoelectromechanical computer was proposed which has acquired urgency as it offers the tantalizing prospect of low power consumption. In spite of some recent experimental effort, a universal electromechanical logic gate based on Boolean algebra has remained beyond reach. To address this, we realise a practical logic device in an electromechanical resonator operated in the non-degenerate parametric amplification regime [2, 3].

Widely used in optics, non-degenerate parametric amplifiers can enable the frequency of a laser to be tuned. Frequency conversion is realised by exploiting the interaction of an intense high frequency pump beam (f_p) with a less intense lower frequency signal beam (f_s) in a crystal with a nonlinearity due for example to the Kerr effect which both amplifies the signal beam as well as generating an idler beam (f_i) where this process conserves energy i.e. $hf_p = hf_s + hf_i$ and h is Planck's constant.

Here we exploit this concept in a tiny mechanical resonator (Fig. 1) where multiple channels of binary information are encoded via the pump as nanometre scale oscillations at different frequencies. The parametrically activated nonlinearity in the mechanical resonator can mix the input binary channels resulting in a rich idler spectrum of output oscillation states that can be used to not only construct all the primary logic gates and multi-bit logic circuits (Fig. 2) but also to execute Boolean logic functions in parallel all in just a single mechanical oscillator. These results suggest that a nanomechanical computer based on these ground breaking techniques could have potentially unrivalled data processing power.

- [1] <http://www.sciencemuseum.org.uk/onlinestuff/stories/babbage.aspx>
 [2] I. Mahboob et al., Nature Commun. **2** (2011) 198.
 [3] I. Mahboob et al., Appl. Phys. Lett. **97** (2010) 253105.

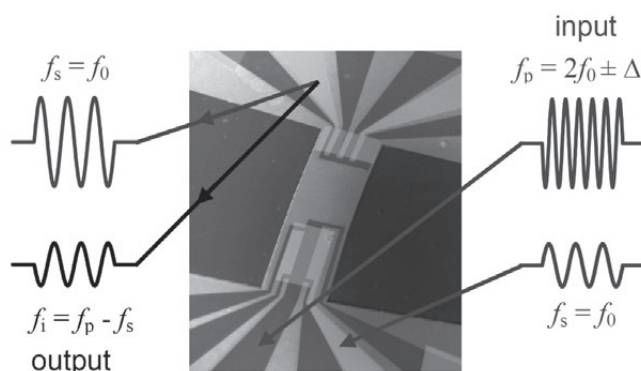


Fig. 1. An SEM image of the parametric amplifier consisting of a doubly clamped beam with an out-of-plane oscillation mode. Application of a.c. bias to the resonator can piezoelectrically induce both harmonic and parametric resonances. Also shown are the input pump and signal excitations and the output amplified signal and idler oscillations.

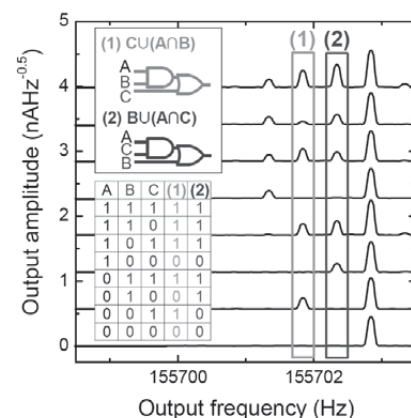


Fig. 2. Application of 3 pumps A, B and C at different pump frequencies results in a rich idler spectrum which can be used to realise multi-bit logic circuits in parallel.

Carrier-Mediated Opto-Mechanical Coupling in GaAs Cantilevers

Hajime Okamoto, Koji Onomitsu, Haruki Sanada*, Hideki Gotoh*,
Tetsuomi Sogawa*, and Hiroshi Yamaguchi
Physical Science Laboratory, *Optical Science Laboratory

Optically induced dynamic backaction in micromechanical systems has recently become the focus of research [1, 2]. Cavity-induced opto-mechanical coupling via radiation pressure or photothermal stress influences the thermal vibration of the mechanical system, leading to amplification and de-amplification of the vibration modes [1, 2]. The vibration amplification is of great interest because it can lead to the self-oscillation of a micromechanical resonator [1, 2]. The de-amplification is of equal interest because it enables cooling of the vibration modes [1, 2]. In contrast, we have recently observed novel opto-mechanical coupling, which does not require any cavities but is based on optical carrier excitation [3, 4]. Here, we report the carrier-mediated opto-mechanical coupling found in *n*-GaAs/*i*-GaAs bilayer cantilevers [Fig. 1(a)].

The carrier-mediated opto-mechanical coupling is based on the strain-assisted opto-piezoelectric effect, which is associated with the separation of electron-hole pairs due to the built-in electric field. Thermal vibration of the [110]-oriented cantilever is amplified by the optical excitation with the near absorption-edge wavelength ($\lambda_{\text{ex}} = 840$ nm at 50 K) and the self-oscillation is induced for the strong excitation ($P_{\text{ex}} > 10$ μW) [Fig. 1(b)]. In contrast, for the [-110]-oriented cantilever, the opto-piezoelectric backaction de-amplifies the vibration because the piezoelectric effect is reversed in the 90-degree rotated orientation [Fig. 1(c)]. This opto-piezoelectric backaction is maximized when the laser wavelength matches the optical absorption edge [4]. This is because the strain-induced change in the optical absorption is maximized at the strain-sensitive absorption edge. This carrier-mediated opto-mechanical coupling has an advantage in compatibility with semiconductor opto-electronics and will also provide a tool for studying the fundamental properties of semiconductors, such as carrier dynamics, strain effects, and carrier-related energy relaxation.

- [1] I. Favero and K. Karrai, *Nature Photon.* **3** (2009) 201.
- [2] C. H. Metzger and K. Karrai, *Nature* **432** (2004) 1002.
- [3] H. Okamoto et al., *Appl. Phys. Express.* **2** (2009) 035001.
- [4] H. Okamoto et al., *Phys. Rev. Lett.* **106** (2011) 036801.

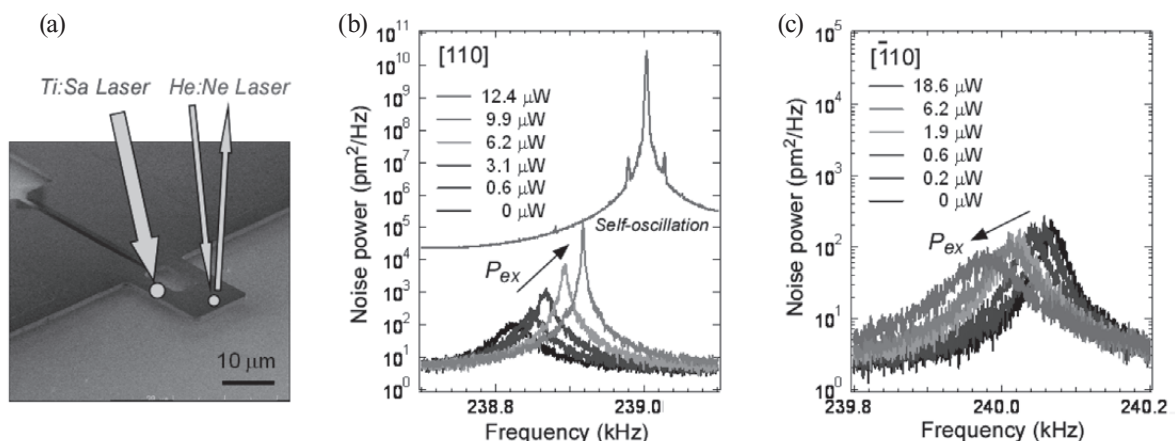


Fig. 1. (a) Scanning electron micrograph of the cantilever. The cantilever consists of 100-nm-thick *n*-GaAs and 200-nm-thick *i*-GaAs. The Ti:Sa cw laser beam is focused on the leg where the larger strain results. The thermal vibration is detected with the He:Ne cw laser beam by laser interferometry. The measurements were done in a vacuum at 50 K. The Ti:Sa laser power dependence of the displacement noise power spectrum for $\lambda_{\text{ex}} = 840$ nm in the (b) [110]-oriented cantilever and (c) [-110]-oriented cantilever.

Voltage-Controlled Group Velocity of Edge Magnetoplasmon in the Quantum Hall Regime

Hiroshi Kamata^{1,2}, Takeshi Ota¹, Koji Muraki¹, and Toshimasa Fujisawa²
¹Physical Science Laboratory, ²Tokyo Institute of Technology

When a two-dimensional electron system is subjected to a strong perpendicular magnetic field, the Lorentz force makes electrons to propagate along the edge of the sample. In the quantum Hall regime, as the Fermi level in the sample interior lies in the gap between the energy levels discretized by the magnetic field, back scattering between channels at opposite edges is prohibited, which makes these edge channels ideal coherent one dimensional channels without dissipation. Electronic analogues of quantum optics experiments using various interferometers defined with edge channels have been demonstrated, allowing one to study coherent transport properties and quantum statistics of electrons. These experiments suggest the possibility of using edge channels as quantum channels, through which quantum states may be transmitted over a macroscopic distance comparable to the device size. To this end, the group velocity of electrons is one important physical parameters to be controlled.

We investigate the group velocity of edge magnetoplasmons (EMPs) in the quantum Hall regime by means of time-of-flight measurement [1]. EMPs generated at $t = 0$ by applying a voltage pulse to the source electrode propagate along the sample edge toward the quantum point contact (QPC). By temporarily opening the QPC at a delay time t_d with another voltage pulse, we are able to selectively detect EMPs arriving at a given time delay t_d as a drain current I_{DS} (Fig. 1). We find that the group velocity of EMPs traveling along the edges defined by a metallic gate strongly depends on the voltage V_G on the gate (Fig. 2). The observed variation of the velocity with V_G can be understood as reflecting the degree of screening provided by the metallic gate, which damps the in-plane electric field and hence reduces the velocity. The degree of screening varies as V_G changes the distance between the gate and the edge channel.

[1] H. Kamata, T. Ota, K. Muraki, and T. Fujisawa, Phys. Rev. B **81** (2010) 085329.

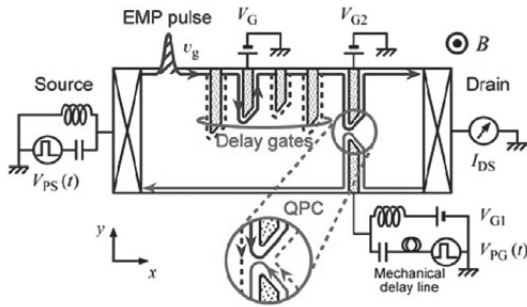


Fig. 1. (a) Schematic illustration of device structure and experimental setup for time-of-flight measurement. A short voltage pulse $V_{PS}(t)$ is applied to the source contact to inject a pulse of EMPs. Another voltage pulse $V_{PG}(t)$ is applied to the QPC to probe the local potential. The time interval between the two voltage pulses is varied using the mechanical delay line. Four delay gates between the source contact and the QPC are used to add extra path length.

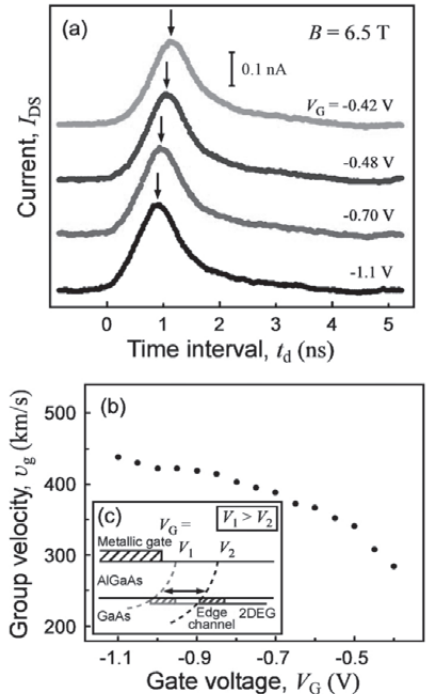


Fig. 2. (a) I_{DS} vs t_d for various V_G . Data are offset for clarity. (b) Group velocity v_g as a function of V_G . (c) Schematic illustrating the cross-sectional view of the sample structure.

Wide-Band Capacitance Measurement on a Semiconductor Double Quantum Dot for Studying Tunneling Dynamics

Takeshi Ota, Toshiaki Hayashi, Koji Muraki, and Toshimasa Fujisawa*
Physical Science Laboratory, *Tokyo Institute of Technology

The electronic properties of a semiconductor quantum dot, that forms a basic for solid-state qubits, can be often well described by a capacitance that characterizes the static and dynamic response of a quantum dot to externally applied voltages. We propose and demonstrate a new experimental technique to measure impedance (both resistance and capacitance) of semiconductor quantum dots in order to study tunneling dynamics [1]. Figure 1(a) schematically shows the experimental setup. A DQD and a nearby quantum point contact (QPC) are formed in a two-dimensional electron gas at the interface of a GaAs/AlGaAs heterojunction by applying negative voltages to surface Schottky metal gates. A square wave $V_{\text{DQD}}(t)$ applied to the DQD induces a single-electron tunneling both on and off and between the dots and the resultant change in the charge state of the DQD $Q_{\text{DQD}}(t)$ modulates the conductance of the QPC. By applying another square wave $V_{\text{QPC}}(t)$ with a relative phase θ to the QPC, we measure the averaged dc current $\langle I_{\text{QPC}} \rangle$ through the QPC by a Lock-in detection. $\langle I_{\text{QPC}} \rangle$ is proportional to the capacitance (conductance) when $\theta = 0$ ($\pi/2$). The capacitance signal appears as a peak or a dip depending on the location of the DQD and the QPC. Figure 1(b) shows the capacitance signal measured at 1 kHz as a function of the gate voltages V_{UR} and V_{UL} . The data reveal a charge stability diagram which forms a honeycomb-shaped structure characteristic of a weakly coupled DQD. In a strongly coupled DQD, the capacitance undergoes a quantum mechanical correction due to the interdot tunnel coupling, and quantum capacitance C_Q is observed. Figure 1(c) shows the variation of C_Q due to interdot tunneling with V_{UC} . As the interdot coupling is weakened by making V_{UC} more negative, the dip becomes sharper. These results suggest that the size and the width of the dip reflect the strength of the quantum mechanical coupling. This C_Q , given by the second derivative, or the curvature, of the energy band E with respect to the gate voltage V_G , i.e., $C_Q \equiv d^2 E/dV_G^2$, is therefore expected to be capable of distinguishing the bonding and antibonding states of single-electron systems or the singlet and triplet states of two-electron systems.

This work was partly supported by SCOPE from the Ministry of Internal Affairs and Communications of Japan.

[1] T. Ota et al., Appl. Phys. Lett. **96** (2010) 032104.

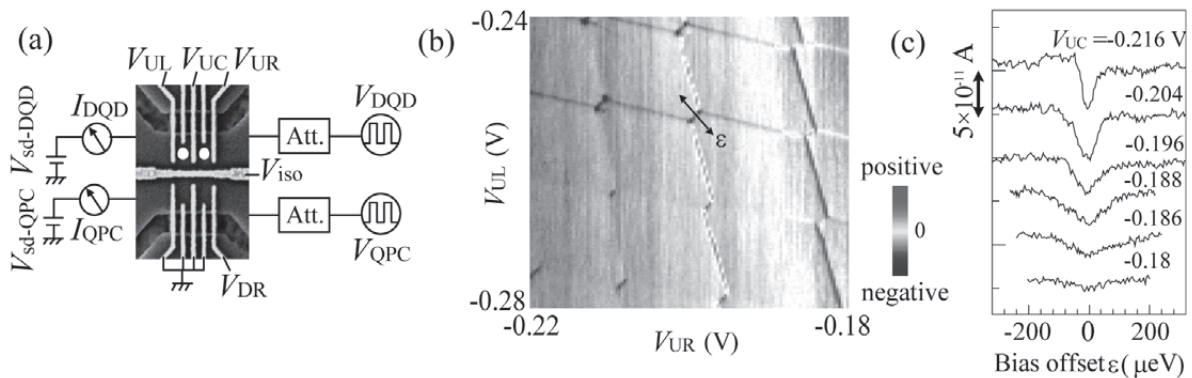


Fig. 1. Schematic illustration of the experimental setup (a), $\langle I_{\text{QPC}} \rangle$ as a function of V_{UL} and V_{UR} (b), $\langle I_{\text{QPC}} \rangle$ as a function of the bias offset ϵ at several V_{UC} (c).

Coherent Operation of a Gap-Tunable Flux Qubit

Xiaobo Zhu, Alexander Kemp, Shiro Saito, and Kouichi Semba
Physical Science Laboratory

The flux qubit is one of the most promising candidates for constructing quantum processors. An upgraded flux qubit, whose gap can be tuned *in situ* by two high bandwidth control lines, gives us two fundamental improvements: "gap control" and " σ_x coupling". Based on these two fundamental improvements many possible applications can be realized, for example, realizing scalable qubus type multi qubits coupling and gate operations with large ON/OFF ratio[1] and σ_x coupling toward demonstration of quantum nondemolition measurement (QND) in solid state device [2].

Recently, we experimentally demonstrated the *in situ* tunability of the gap of a superconducting flux qubit, which was achieved by replacing the smallest Josephson junction of the qubit with a DC-SQUID. By adding pulses via a local control line we can tune the gap over a range of several GHz on a nanosecond time scale (Fig.1). The variation of the persistent current and the gap with the control pulses is consistent with the simulation.

Rabi oscillations between the ground state and the first excited state are a primary demonstration of a single qubit coherent operation. In Fig. 2(a), we show Rabi oscillations obtained at the degeneracy point. We set the voltage level of the two control lines to the degeneracy point of a dispersion relation, and varied the length of the microwave pulse resonant with the qubit, i.e., the gap frequency. After above sequence, the qubit state is measured by applying a measurement pulse. We repeated the whole sequence 2000 times to detect the relative occupation of the ground state and the excited state. We varied the amplitude of the microwave, and verified the linear dependence of the Rabi frequency on the microwave amplitude as shown in Fig. 2(b), which is a signature of the Rabi process [3].

[1] Y. D. Wang, A. Kemp, K. Semba, Phys. Rev. B **79** (2009) 024502.

[2] Y. D. Wang, X. Zhu, and C. Bruder, Phys. Rev. B **83** (2011) 134504.

[3] X. Zhu, A. Kemp, S. Saito, and K. Semba, Appl. Phys. Lett. **97** (2010) 102503.

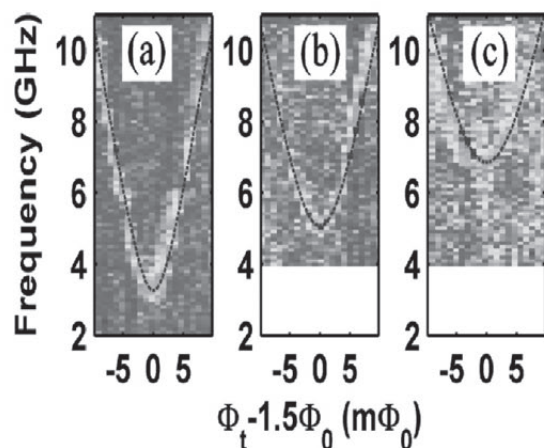


Fig. 1. Spectroscopies with different gap value (a) 3GHz, (b) 5GHz, (c) 7GHz by applying *in situ* pulse at fixed magnetic field.

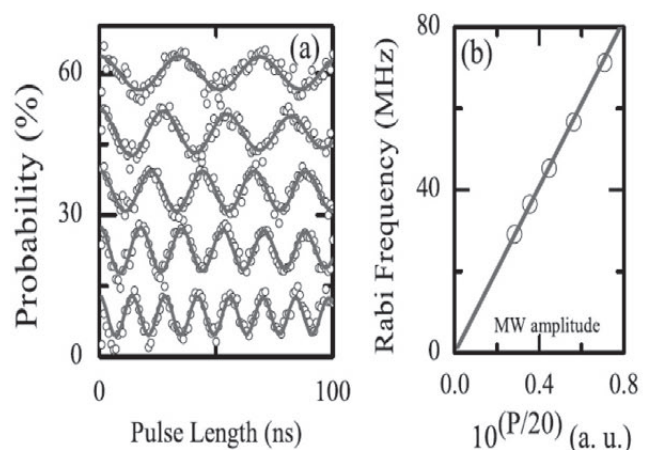


Fig. 2. (a) Rabi oscillations at one degeneracy point for five different microwave powers. (b) Linear dependence of the Rabi frequency on the microwave amplitude.

Generation of Non-Classical Microwave Photon States in an Inductor-Capacitor Resonator Coupled to a Superconducting Flux Qubit

Kosuke Kakuyanagi, Shiro Saito, Hayato Nakano, and Kouichi Semba
Physical Science Laboratory

To realize quantum memories for quantum computation, we need to establish quantum information transfer and the generation of a photon number state (especially a one-photon state). However it is difficult to generate a photon number state because the method, which excites an LC resonator by using a resonant microwave, forms a classical coherent state. So, we attempt to generate a non-classical photon state by transferring a photon from a superconducting qubit to an LC resonator.

The LC resonator, which is constructed from a line inductor and a capacitor, surrounds a superconducting flux qubit (Fig. 1). The magnetic coupling energy between the flux qubit and the LC resonator is 360 MHz. A large coupling energy is one of the advantages of using a superconducting qubit. In this LC resonator and flux qubit system, we shift the external magnetic field non-adiabatically, after realizing the excited qubit state. By tuning the resonant condition of the LC resonator and qubit, we generate a photon oscillation, which is called a vacuum Rabi oscillation. Time domain control of this quantum oscillation makes it possible to transfer a photon from a qubit to an LC resonator. By repeating this process, we can transfer photons one by one. The ideal photon state achieved using this method becomes the photon number state. Period time of quantum oscillation of this system depends on the photon number, so we can obtain information about the photon distribution of the LC resonator by analyzing the time domain oscillation.

Figure 2 shows the photon distribution results when we transfer one and two photons to the LC resonator. Energy relaxation and the imperfection of the control pulses mean that this photon distribution is different from the pure photon number state. However, we succeeded in generating a non-classical photon distribution, which is clearly different from a classical Poisson distribution [1]. This is the result of using the LC resonator's quantum characteristics, so we can expect the development of quantum memories by using high-Q resonators.

[1] K. Kakuyanagi et al., *Appl. Phys. Express* **3** (2010) 103101.

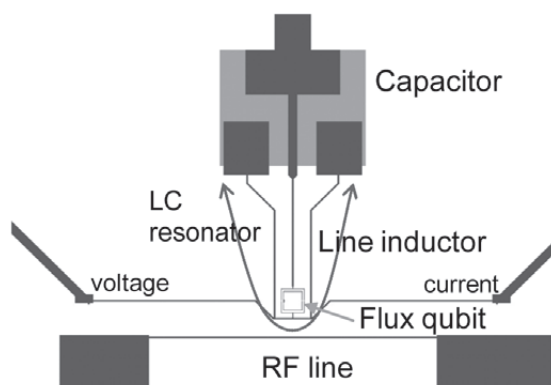


Fig. 1. Sample design of LC resonator and superconducting flux qubit.

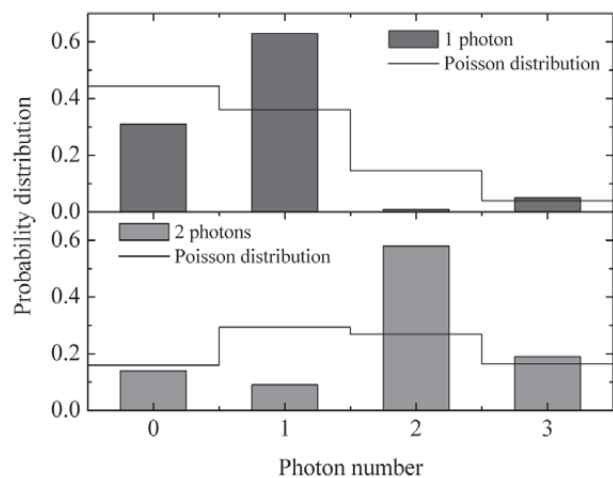


Fig. 2. Corresponding Poisson distributions and results of photon distributions of LC resonator when we transfer one and two photons.

Quantum Zeno Effect with a Superconducting Qubit

Yuichiro Matsuzaki, Shiro Saito, Kosuke Kakuyanagi, and Kouichi Semba
Physical Science Laboratory

Quantum Zeno effect (QZE) is one of fascinating phenomena which quantum mechanics predict. A sequence of projective measurements to an unstable system can suppress the decay process of the state [1]. This phenomenon will be observed if the time interval of projective measurements is sufficiently small and the decay behavior in the time interval is quadratic.

The difficulty for the experimental demonstration of QZE is to observe such quadratic decay behavior experimentally. The time region to show such quadratic behavior is comparable with the correlation time of the noise, which is usually much shorter than typical time resolution of a measurement apparatus in the current technology. After showing the quadratic decay, unstable system shows an exponential decay and QZE does not occur through projective measurements to a system which decays exponentially. Due to such difficulty, there was only one experimental demonstration to suppress the decay process of an unstable state by projective measurements [2].

We suggest a way to demonstrate QZE experimentally with a superconducting qubit [3] (see Fig. 1). For a superconducting qubit, the quadratic decay can be observed in an experiment due to $1/f$ noise whose correlation time is infinite unlike the other typical noise sources where f denotes a frequency. Although a relaxation process causes an exponential decay to the superconducting qubit, by solving a master equation, we have found that one can still increase the success probability to project the state into a target subspace through frequent selective measurements as long as the relaxation time is sufficiently longer than the dephasing time (see Fig. 2). Also, we have shown that, with experimentally realizable parameters, it is possible to observe the suppression of the dephasing caused by $1/f$ noise by nonselective measurements. Although these results are theoretical, they have been obtained with practical experimental conditions and therefore there will soon be experimental demonstration.

[1] B. Misra et al., *J. Math. Phys.* **18** (1997) 756.

[2] M. C. Fischer et al., *Phys. Rev. Lett.* **87** (2001) 040402.

[3] Y. Matsuzaki et al., *Phys. Rev. B.* **82** (2010) 180518.

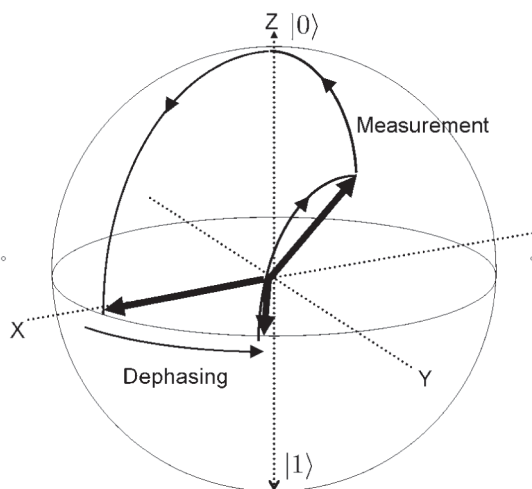


Fig. 1. A schematic of a quantum state to show how QZE is observed with a superconducting qubit.

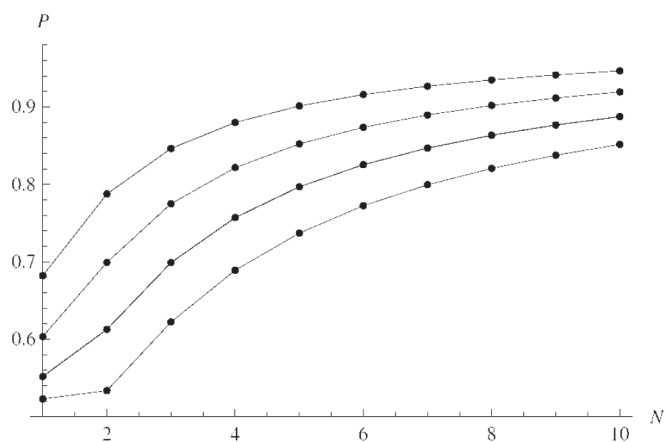


Fig. 2. A success probability of projections under the decoherence for time interval of 20 (top line), 25, 30, 35 ns (bottom line). N and P denote the number of measurements for the time and a success probability, respectively.

Evaluation of Spin Polarization in $p\text{-In}_{0.96}\text{Mn}_{0.04}\text{As}$ Using Andreev Reflection Spectroscopy Including Inverse Proximity Effect

Tatsushi Akazaki¹, Takehito Yokoyama², Yukio Tanaka³,
Hiro Munekata², and Hideaki Takayanagi^{4,5}

¹Physical Science Laboratory, ²Tokyo Inst. Tech., ³Nagoya Univ.,
⁴Tokyo Univ. of Science, ⁵NIMS-MANA

In superconductor/ferromagnet (S-F) junctions, new quantum phenomena can be expected from the interplay between the superconductivity and the spin polarization of the ferromagnet. This interplay allows us to determine experimentally the spin polarization of carriers P in a ferromagnet using Andreev reflection spectroscopy [1]. However, it is inferred that, in an S-F junction, the pair potential Δ in a superconductor is weakened as a result of the penetration of the exchange field from a ferromagnet into a superconductor, which is called the inverse proximity effect. This interesting deliberation has motivated us to study the influence of the inverse proximity effect on spin-polarized carrier transport across the S-F interface as well as the estimation of the P value.

We fabricated Nb/ferromagnetic semiconductor $p\text{-In}_{0.96}\text{Mn}_{0.04}\text{As}$ junctions as shown in Fig. 1. Below ~ 10 K, $p\text{-In}_{0.96}\text{Mn}_{0.04}\text{As}$ becomes ferromagnetic, as evidenced by the hysteretic transverse resistance caused by the anomalous Hall effect. Figure 2 shows the dI/dV - V characteristics of a Nb/ $p\text{-In}_{0.96}\text{Mn}_{0.04}\text{As}$ junction at various temperatures. Below the T_C of Nb (~ 8.2 K), a conductance reduction occurs within the bias voltage that is comparable to the Nb superconducting energy gap. A rather moderate slope in the differential conductance curves within the gap region indicates the partial suppression of the Andreev reflection caused by spin-polarized carriers in $p\text{-In}_{0.96}\text{Mn}_{0.04}\text{As}$. The P value in $p\text{-In}_{0.96}\text{Mn}_{0.04}\text{As}$ has been extracted by fitting the measured differential conductance curves with a newly modified Blonder-Tinkham-Klapwijk model [2] with both spin polarization and the inverse proximity effect as shown in Fig. 3. The extracted P value is $P = 0.725$ at 0.5 K, and it decreases gradually with increasing temperature.

This work was supported in part by the "Topological Quantum Phenomena" KAKENHI on Innovative Areas from MEXT.

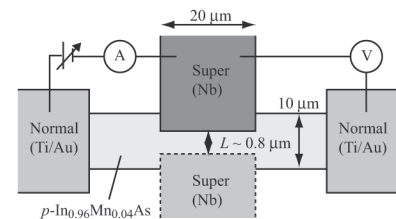


Fig. 1. Schematic diagram of a Nb/ $p\text{-In}_{0.96}\text{Mn}_{0.04}\text{As}$ junction.

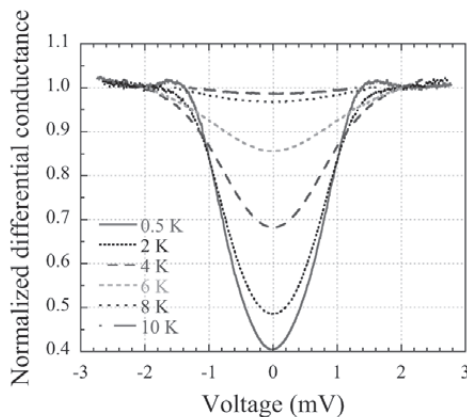


Fig. 2. Normalized dI/dV - V characteristics at various temperatures.

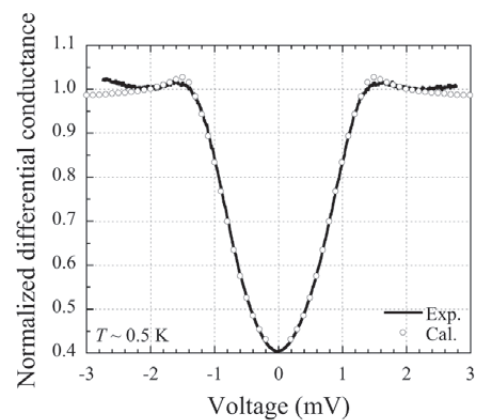


Fig. 3. Comparison of the normalized dI/dV - V characteristics calculated from our model (open circles) with experimental data (thick solid line) at 0.5 K. The values used in the calculation are $Z = 0.25$ and $P = 0.725$.

Photoluminescence Spectroscopy of the Low-Density Two-Dimensional Electron System in Electric Fields

Masumi Yamaguchi, Shintaro Nomura*, Hiroyuki Tamura, and Tatsushi Akazaki
Physical Science Laboratory, *Univ. of Tsukuba

At low temperature, the photoluminescence (PL) spectrum of a two-dimensional electron system (2DES) reflects the potential fluctuation. We have studied the random-potential screening across the metal-insulator transition of the 2DES formed in a double-gated GaAs quantum well [1]. Here, we investigated the PL spectra of 2DES-hole emission in various perpendicular electric fields and found that the difference in the PL linewidth in electric fields decreases with electron density [2].

As shown in Fig. 1, the emission energy of PL decreases with perpendicular electric fields due to the quantum confined Stark effect (QCSE). In addition, the PL linewidth increases with perpendicular electric fields due to the monolayer well-width fluctuation since the QCSE energy shift depends on the well width. Below $n_e \sim 4 \times 10^{10} \text{ cm}^{-2}$, 2DES is highly inhomogeneous because of the Coulomb random potential of remote charge. In this case, the PL linewidth, which is the superposition of individual emission energies at different positions, increases with perpendicular electric fields. On the other hand, when the electron state extends to an area larger than the spatial range of the well-width fluctuation, the electric field dependence of PL linewidth disappears because the electrons feel the spatially averaged potential.

Figure 2 shows the slopes of the PL linewidth against perpendicular electric fields as a function of electron density. Below $4 \times 10^{10} \text{ cm}^{-2}$, the slope decreases with increasing electron density and becomes almost zero above $6 \times 10^{10} \text{ cm}^{-2}$. This reflects the spatial extension of the 2DES over the Coulomb disorder and the well-width fluctuation range as electron density increased.

This work was supported by KAKENHI.

[1] M. Yamaguchi et al., Phys. Rev. Lett. **100** (2008) 207401.

[2] M. Yamaguchi et al., Physics Procedia **3** (2010) 1183.

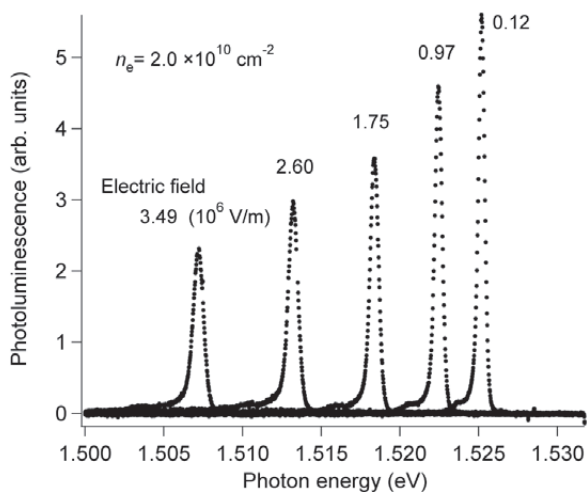


Fig. 1. Photoluminescence spectrum at $n_e = 2 \times 10^{10} \text{ cm}^{-2}$ for various perpendicular electric fields.

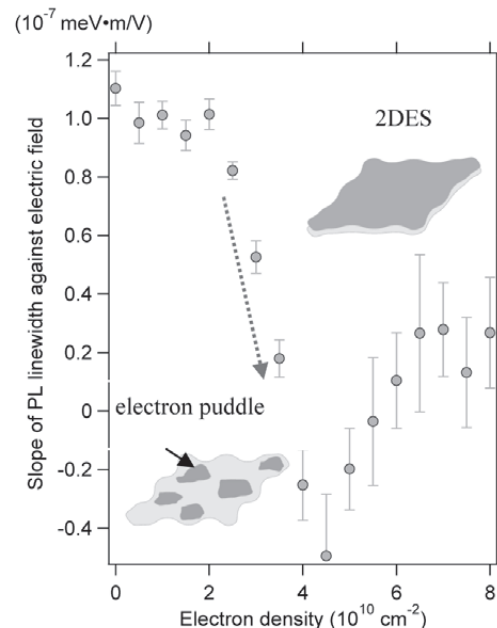


Fig. 2. Electron density dependence of the slope of the PL linewidth change against perpendicular electric fields.

Single-Photon Detection Using Magnesium Diboride Superconducting Nanowire at Telecommunication Wavelength

Hiroyuki Shibata, Hiroki Takesue, Toshimori Honjo, Tatsushi Akazaki*, and Yasuhiro Tokura
Optical Science Laboratory, *Physical Science Laboratory

Magnesium diboride (MgB_2) is a next generation superconducting material because of its highest $T_c=39$ K among intermetallic compounds and of its simple crystal structure with only two elements. We have reported that it is possible to grow MgB_2 ultra-thin films using molecular beam epitaxy (MBE) with a precise control of evaporation ratio of Mg and B vapors [1]. We have also reported that it is possible to fabricate nano-patterns of MgB_2 by the liftoff process using amorphous carbon as a resist, which can bear at high temperature during MgB_2 deposition [1]. Recently, we have fabricated an MgB_2 nanowire with the dimension of 100-nm-width and 10-nm-thick and have demonstrated that the nanowire can detect single-photons in the visible to infrared wavelength range [2].

Figure 1 shows the atomic force microscopy (AFM) image of MgB_2 nanowire. The uniform shape of the nanowire demonstrates that the liftoff process works well. The transport measurement also showed that the nanowire has no damage during nano-fabrication process. The single-photon detection capability can be confirmed by investigating the statistics regarding the number of detected signals and the average number of photons illuminating the nanowire. When the illumination is a weakly coherent light source with a Poisson distribution, the probability of detecting one photon is proportional to the average number of photons μ . Figure 2(a) shows the μ dependence of the number of detected signals at wavelength of 405 nm. The dependence is linear, confirming the single-photon detection capability of the nanowire. At 1560 nm, quadratic dependence is observed in Fig. 2(b) in the low bias region. This indicates that the energy of single-photon at 1560 nm is not enough to make electric signals and more than two-photons are necessary to make signals. The dependence changes linear as the bias increases higher, demonstrating the single-photon detection capability of the nanowire even at 1560 nm. We will try to fabricate a single-photon detector for the quantum information and quantum optics using MgB_2 nanowire.

This work was supported by KAKENHI.

[1] H. Shibata et al., IEEE Trans. Appl. Supercond. **19** (2009) 358; H. Shibata et al., Physica C **470** (2010) S1005.

[2] H. Shibata et al., Appl. Phys. Lett. **97** (2010) 212504.

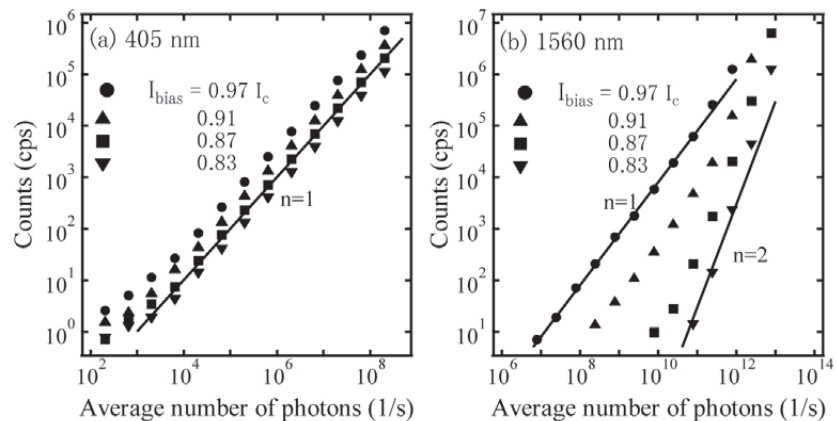
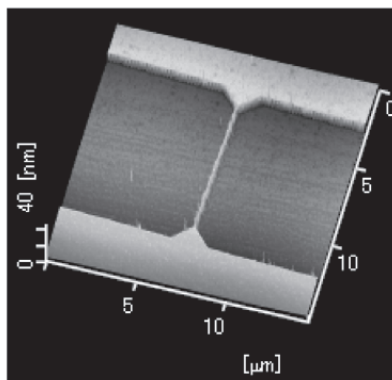


Fig. 1. AFM image of a MgB_2 nanowire.

Fig. 2. Optical detection characteristics of MgB_2 nanowire at (a) 405 and (b) 1560 nm. I_{bias} is a bias current and I_c is a critical current. $n=1$ means linear dependence and $n=2$ means quadratic dependence.

Tokyo QKD Network

Kiyoshi Tamaki, Toshimori Honjo, Hiroki Takesue, and Yasuhiro Tokura
Optical Science Laboratory

NTT, NEC, and Mitsubishi electric, which are funded by NICT, developed each of their Quantum Key Distribution (QKD) system, and connected in Tokyo these systems as well as QKD systems brought by AIT, Id quantique, Toshiba Research Europe, which forms Tokyo QKD Network.

QKD is a way to distribute the so-called key. The key is a random bit string whose information is not leaked to unauthorized parties, and the key is used for authorized parties to communicate each other without leakage of its information. In order to prevent eavesdropping, QKD employs the fact that no one can be against the law of nature, including the so-called quantum mechanics. More attentions have been paid to this cryptography which is unbreakable given the users' devices operate as the theory imposes.

Tokyo QKD network consists of six nodes over the optical communication testbed network, JGN2plus (Fig. 1), and two of the nodes can generate the key being fast enough for the live transfer of a video data. NTT was in charge of the longest link of 90 km between Koganei and Otemachi and back, and we have successfully realized 2 kbps of the key generation rate. We have developed a system for the Differential Phase Shift QKD (DPS-QKD) [1], which was proposed jointly by NTT and Stanford University. This protocol features its simplicity of the system configuration, and thus it is easy to be implemented. We have used Field-Programmable Gate Array for high-speed random number generation with 1GHz clock, fast signal generation, and fast memory access, and also we have implemented polarization feedback controller to eliminate the polarization dependency of superconducting single photon detectors developed by NICT. This system outputs the "sifted key", from which the key to be used over the optical network is distilled via some data processing by the key distillation engine developed by NEC.

Thanks to these attempts for the stabilization and speeding-up, we have achieved stable generation of the sifted key over 8 days with about 18 kbps of the generation rate as well as 2 kbps of the secure key generation rate (Fig. 2) [2].

This work was in part supported by NICT.

[1] K. Inoue et al., Phys. Rev. A **68** (2003) 022317.

[2] M. Sasaki et al., Opt. Express **19** (2011) 10387.

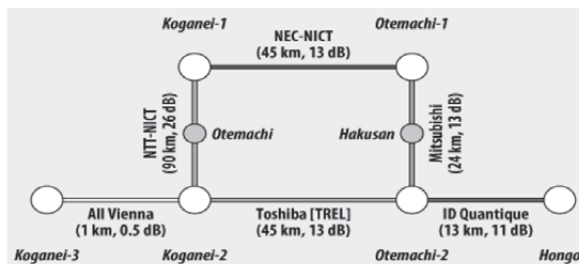


Fig. 1. Topology of the network.

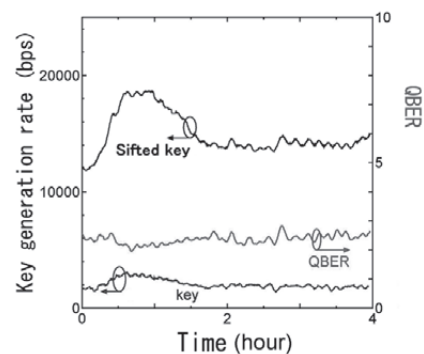


Fig. 2. QBER, sifted and key generation rate.

Kondo Effects and Current Shot Noise in a Double Quantum Dot

Toshihiro Kubo and Yasuhiro Tokura
Optical Science Laboratory

The various kinds of Kondo effect not seen in conventional metallic systems have been revealed in semiconductor quantum dot (QD) systems since the many parameters are experimentally tunable [1]. In a double quantum dot (DQD), the pseudospin state is represented as a state with an electron in either of two capacitively coupled QDs. We have theoretically investigated the pseudospin Kondo effect without spin degree of freedom [2].

In this work, we consider the spin degree of freedom and study the spin/pseudospin Kondo effects in a laterally coupled DQD as shown in Fig. 1. at zero temperature using the slave-boson mean-field theory based on the nonequilibrium Green's function method. The notation (N_1, N_2) in Figs. 2 and 3 indicates the number of electrons in two QDs. Figure 2 shows the linear conductance on the charge stability diagram. In the pseudospin Kondo regime such as the boundary between $(1,0)$ and $(0,1)$, we cannot observe the characteristic property. Thus, it is difficult to capture the signature of the pseudospin Kondo effect by standard transport measurements. In contrast, we plot the zero-frequency current shot noise on the charge stability diagram under low bias voltage condition ($eV_{SD}/\eta\Gamma=0.1$, where Γ is the coupling strength between the reservoir and the QD) in Fig. 3. In contrast to the linear conductance, the current shot noise can provide a clear signature of the pseudospin Kondo effect, namely the current shot noise is maximal in the pseudospin Kondo regime [3]. So far we consider the DQD without coherent indirect coupling [4], in the following, we examine effects of the coherent indirect coupling on the spin Kondo effect. When each QD holds just one electron, the fourth-order perturbation theory of the tunneling process between the reservoir and QDs gives rise to the antiferromagnetic kinetic exchange coupling. Although the effect of coherent indirect coupling had been discussed only on the orbital degree of freedom, we clarified this antiferromagnetic exchange coupling on the spin degree of freedom for the first time. Consequently we found that the spin Kondo effect in $(1,1)$ region is suppressed by such an antiferromagnetic exchange coupling.

This research was supported by ICORP of Japan Science and Technology Agency, FIRST of Government of Japan, and KAKENHI.

- [1] S. Sasaki et al., Nature **405** (2000) 764.
- [2] T. Kubo et al., Phys. Rev. B **77** (2008) 041305(R).
- [3] T. Kubo et al., Phys. Rev. B **83** (2011) 115310.
- [4] T. Kubo et al., Phys. Rev. B **74** (2006) 205310.

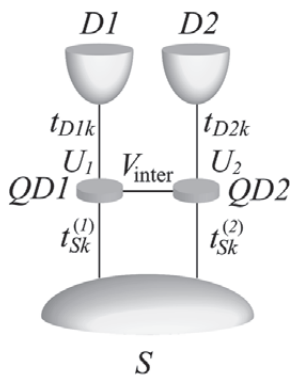


Fig. 1. Schematic diagram of the laterally coupled double quantum dot.

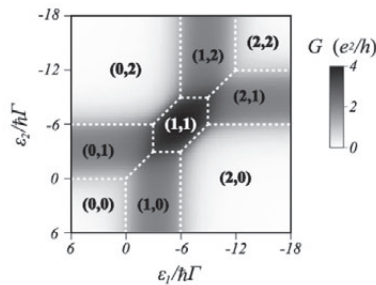


Fig. 2. Linear conductance on the charge stability diagram.

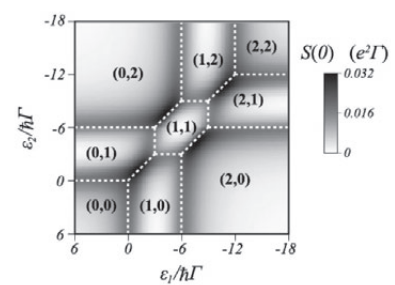


Fig. 3. Zero-frequency current shot noise on the charge stability diagram ($eV_{SD}/\eta\Gamma=0.1$).

Cavity Quantum Electrodynamics Using Single Quantum Dot

Takehiko Tawara, Hidehiko Kamada, and Stephen Hughes*
Optical Science Laboratory, *Queen's University

Cavity quantum electrodynamics (cQED) has been intensively studied using a solid-state two-level system, and has found use for quantum information devices such as those employing nonlinearities generated by single photons and the quantum state exchange between light and matter. In solid-state cQED, however, the environment that surrounds a two-level system is quite different from that of an atom trapped in a vacuum, and so the interpretation of its optical response is abstruse [1]. In this study, we explore a novel optical response in solid-state cQED in weak and strong coupling regimes, and investigate the corresponding mechanisms.

We used a self-assembled semiconductor quantum dot (QD) as a two-level system that is embedded in a 2D photonic crystal nanocavity. Figure 1 shows a series of PL spectra of a QD exciton (X) and the cavity mode (C) in a weak coupling regime. As the temperature increases, these two peaks experience a continuous redshift thereby reducing the relative energy separation. However, surprisingly, as the two peaks approach one another near the crossover, the cavity modes clearly undergo a blueshift toward the exciton resonance (mode attraction) [2]. In contrast, the PL spectrum in a strong coupling regime exhibits Rabi splitting with anti-crossing dispersion (Fig. 2). When the excitation power is increased, we observe that the Rabi splitting vanishes although anti-crossing is maintained. We analyzed both curious phenomena theoretically in weak and strong coupling regimes. As the result, we proved that these peculiar phenomena in solid-state cQED arise from the large exciton dephasing and the optical radiation characteristics of a 2D photonic crystal cavity [3].

This work was partially supported by the Strategic Information and Communications R&D Promotion Programme (SCOPE) of Japan.

[1] For example, K. Hennessy et al., *Nature* **445** (2007) 896.

[2] T. Tawara et al., *Opt. Express* **18** (2010) 2719.

[3] S. Hughes et al., *Opt. Express* **17** (2009) 3322.

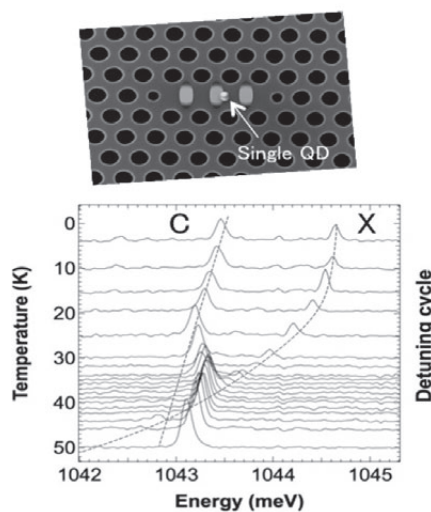


Fig. 1. Series of PL spectra as a function of temperature in weak coupling regime.

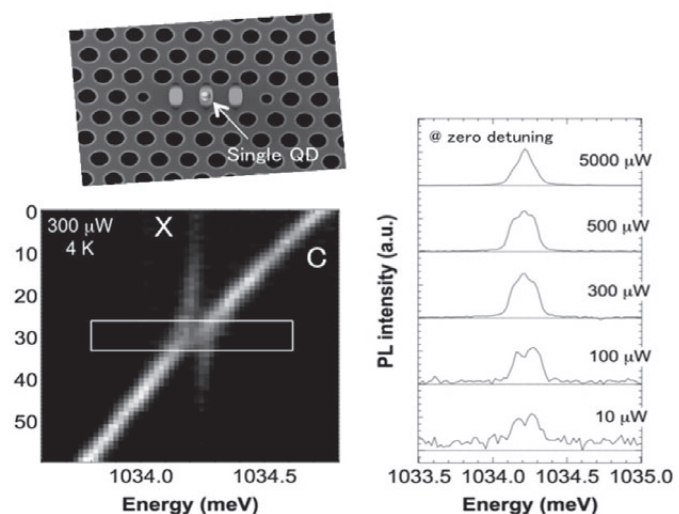


Fig. 2. PL color map and PL spectra at zero detuning with various excitation powers in strong coupling regime.

Nanowires Laterally Grown on GaAs Substrates in the Vapor-Liquid-Solid Mode

Guoqiang Zhang, Kouta Tateno, Hideki Gotoh, and Tetsuomi Sogawa
Optical Science Laboratory

Semiconductor nanowires (NWs) have attracted much attention because of their exceptional versatility and potential for a wide range of applications, from electronics and photonics to biochemistry and medicine [1]. There are two main approaches to the integration of NW-based devices: (1) using freestanding NWs epitaxially grown on a patterned substrate; (2) using an *ex-situ* assembly method designed to align NWs removed from the grown substrate and dispersed on another substrate. The former approach is preferable because of the contamination that occurs during the *ex-situ* assembly process with the latter approach. However, a freestanding structure is very difficult to use as regards electrode formation. The most attractive way to integrate and extend the applications of NW-based devices is to grow the NWs laterally on the substrates with an *in-situ* process. In the current work, we developed a technique for growing lateral GaAs NWs on GaAs (311)B and (001) substrates in the vapor-liquid-solid (VLS) growth mode and demonstrated its high controllability in terms of size, site, and composition [2, 3].

We used Au nanoparticles to catalyze the NW growth in the VLS mode. First, we investigated lateral GaAs NWs grown on a (311)B substrate under optimized growth conditions in a metalorganic vapor phase epitaxy system. Figure 1 shows a cross-sectional transmission electron microscopy (TEM) image of a lateral GaAs NW. There is a Au nanoparticle at the tip of the NW, indicating that the NW is grown in the Au-catalyzed VLS mode. This enables us to control their size and density by using size- and density-selective Au colloidal nanoparticles. We grew the site-specific lateral NW array by using a lithographically defined Au dot array. Figure 2 shows an atomic force microscopy (AFM) image of the array. To form heterostructures for bandgap engineering in the lateral NWs, we incorporated indium (In) during the growth and confirmed the realization of lateral InGaAs NWs [3]. We expect that the planar NW structure will provide new opportunities and new functionalities for the development of electronic devices and highly efficient photonic devices.

[1] L. Samuelson, *Mater. Today* **6** (2003) 22.

[2] G. Zhang, K. Tateno, H. Gotoh, and H. Nakano, *Nanotechnology* **21** (2010) 095607.

[3] G. Zhang, K. Tateno, H. Gotoh, and T. Sogawa, *Appl. Phys. Express* **3** (2010) 105002.

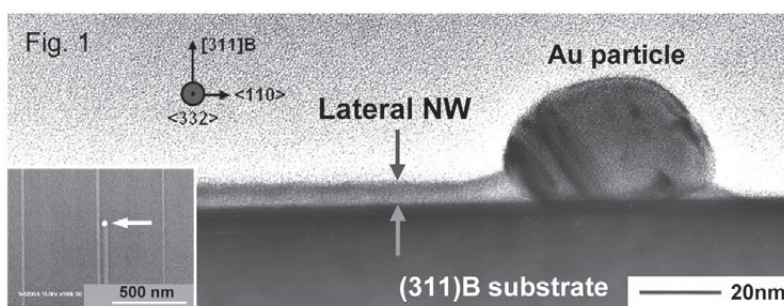


Fig. 1. Cross-sectional TEM image of lateral GaAs NWs on (311) B substrate. Note that there is a Au particle at the lateral NW tip. The arrow in the inset, which is a top-view SEM image of lateral NWs, indicates a Au particle at the NW tip.

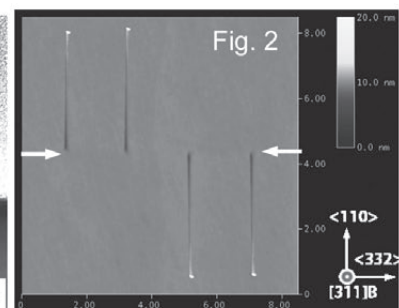


Fig. 2. AFM image of lateral GaAs NWs. Note that the Au particles moved from the initial position, indicated by the white arrows, to the NW tips after the growth.

Coherent Phonons in Metallic Single-Walled Carbon Nanotubes

Keiko Kato, Katsuya Oguri, and Tetsuomi Sogawa
Optical Science Laboratory

Single-walled carbon nanotubes (SWCNT) become either metallic or semiconducting depending on their structure (i.e., chirality). Metallic SWCNTs exhibit ballistic transport due to their quasi-one-dimensional structure. However, electron scattering by optical phonons sets the ultimate limit for high field ballistic transport. To employ metallic SWCNTs as future electronic devices, we must understand the phonon to allow us quantify the interaction between carriers and phonons. Ultrashort laser pulses, whose pulse duration is shorter than the lattice vibration period, make it possible to achieve the real-time observation of lattice oscillation, that is, coherent phonons. Most SWCNTs contain a broad distribution of chiralities. Thus, it is difficult to obtain detailed information or control SWCNTs with a specific chirality because SWCNTs with different chiralities are excited simultaneously in a mixed sample. By using a separation scheme [1], we are able to report ultrafast carrier and coherent phonon dynamics in metallic SWCNTs [2].

Time-resolved reflectivity was measured with a sub-10-fs laser pulse, whose wavelength was centered on 780 nm. Figure 1 shows the time-resolved reflectivity of metallic SWCNTs. At a zero delay-time, a sharp response originating from the excitation of free carriers appears and decays within 30 fs through carrier-carrier scattering. Then, an oscillatory signal, induced with coherent phonons, follows the carrier response (inset in Fig. 1). A Fourier transform analysis reveals that the oscillation originates from coherent phonons of (i) the radial breathing mode, (iii) the G mode, and (ii) even the D mode, which originates from defects in SWCNTs (Fig. 2). The G mode consists of several peaks corresponding to the transverse and longitudinal optical phonon modes for the peaks with the higher and lower frequencies, respectively. The longitudinal phonon exhibits an asymmetric shape due to the interaction between coherent phonons and free carriers. With the separation of metallic SWCNTs from the mixed sample, we identified ultrafast dynamics of free carriers and the electron-phonon coupling.

This work was partly supported by KAKENHI.

[1] K. Yanagi et al., *Appl. Phys. Express* **1** (2008) 034003.

[2] K. Kato et al., *Appl. Phys. Lett.* **97** (2010) 121910.

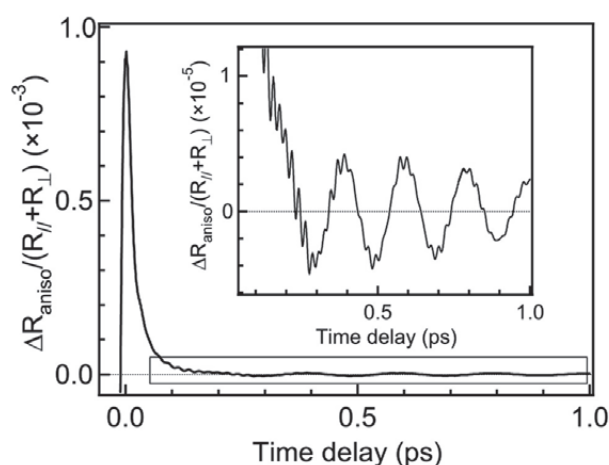


Fig. 1. Time-resolved reflectivity of metallic SWCNTs. Inset shows enlarged graph.

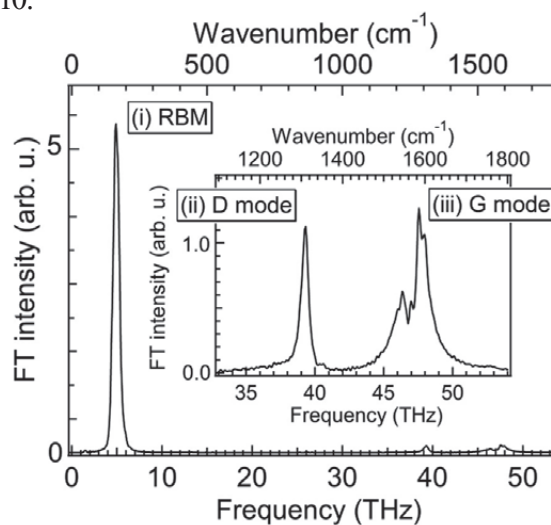


Fig. 2. Fourier power spectrum of time-resolved reflectivity in metallic SWCNTs. Inset shows enlarged graph for D and G modes.

High- Q One-Dimensional Photonic Crystal Nanocavity in a Silicon/SOI Platform

Eiichi Kuramochi, Takasumi Tanabe, Laurent-Daniel Haret,
Hideaki Taniyama, and Masaya Notomi
Optical Science Laboratory

It is well known that a suitably designed chain of submicron holes in a silicon submicron wire-like waveguide fabricated on a silicon-on-insulator (SOI) substrate acts as a nanocavity. It belongs to one-dimensional (1D) photonic crystal (PhC) nanocavities and has attracted attention because it has the simplest design and smallest footprint. However, compared to two-dimensional (2D) PhC nanocavities, which have been highly developed and widely used, the 1D nanocavities have a relatively poor quality factor (Q). In this study, applying the mode-gap confinement approach, which had achieved great success in 2D nanocavities, we found solutions for realizing an ultrahigh Q value in a 1D nanocavity [1].

We studied 1D nanocavities consisting of rectangular (R) and circular holes (C). The buried oxide (BOX) layer underneath the nanocavity was removed in an air-bridge structure (AB) and preserved in a SOI structure. The size of the holes was continuously modulated to generate a mode-gap barrier. Electro-magnetic simulations using the 3D finite-domain time-difference (FDTD) method demonstrated that both structures held ultrahigh Q values exceeding 10^8 and that the C nanocavities had a modal volume (V) smaller than $1(\lambda/n)^3$ (Fig. 1) [1, 2]. Note that even in a SOI structure, our design allows an ultrahigh Q of $\sim 10^8$, which is a unique feature of the 1D nanocavity. These numerical predictions were experimentally demonstrated by measured Q of 3.6×10^5 in the SOI C and 7.2×10^5 in AB C nanocavities (Fig. 2) [2].

Since air acts as thermal insulator, a 1D AB nanocavity has a considerably large heat resistance, which was demonstrated by numerical simulation. In such a nanocavity, thermo-optic nonlinearity is enhanced greatly. We observed the lowest thermo-optic bistability onset power of $1.6 \mu\text{W}$ in a AB R nanocavity (Fig. 3) which had a high optical Q of 2.2×10^5 [3]. Considering the great structural difference between the 1D and the 2D nanocavities, we can expect unique advantages and applications of the former.

This work was partly supported by CREST of Japan Science and Technology Agency.

- [1] M. Notomi et al., *Opt. Express* **16** 11095 (2008).
[2] E. Kuramochi et al., *Opt. Express* **18** 15859 (2010).
[3] L. D. Haret et al., *Opt. Express* **17** 21108 (2009).

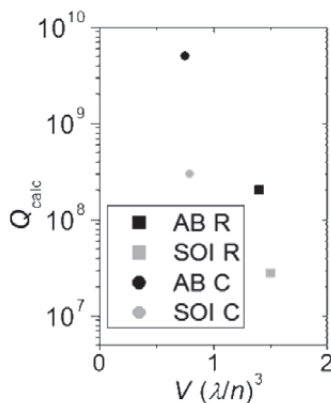


Fig. 1. Calculated Q and V .

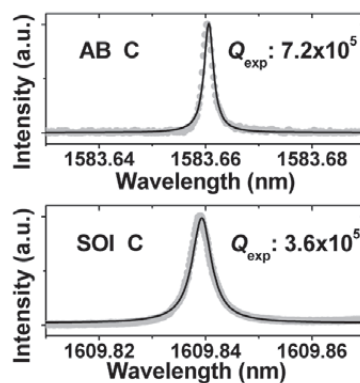


Fig. 2. Spectra of high- Q mode in the nanocavities.

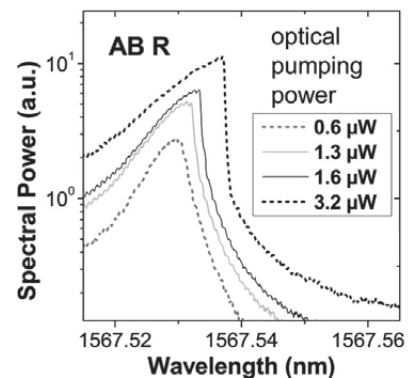


Fig. 3. Thermo-optic bistability onset of a nanocavity mode.

GPGPU Acceleration of the FDTD Calculation

Hideaki Taniyama, Takashi Shimokawabe*, Takayuki Aoki*, and Masaya Notomi
Optical Science Laboratory, *Tokyo Institute of Technology

Finite-Difference Time-Domain (FDTD) method of Maxwell equation is widely used and is recognized as a powerful tool in the study of optical nanostructures. Generally, FDTD simulation requires large amount of memories and long computing time. Therefore, it cannot be used for the calculation of large structures. Recently, the General-Purpose Graphics Processing Unit (GPGPU) featuring massive parallelism and high memory bandwidth has been used for the acceleration in some supercomputers. We try to use GPU as an accelerator of FDTD calculation, to accelerate the FDTD computation and overcome their limitation.

The FDTD calculation requires large memory access in the time integration step of electromagnetic fields. The bottle-neck of FDTD calculation lies in slow memory transfer between main-memory and CPU. On the other hand, a memory bandwidth between GPU and VRAM is high. This suggests the possibility of greatly accelerating the speed of computation by using GPU. To take full advantage of the high memory bandwidth of GPU, we must minimize data transfer between CPU and GPU, because their data transfer costs much of the computation time and counteracts speedup effect of GPU.

We use CUDA 3.1, which is an integrated development environment for NVIDIA's GPGPU. For GPUs, we use NVIDIA's Tesla C1060 and GeForce GTX 480, and for CPU we use Xeon/W3580 3.33 GHz. To estimate the acceleration effect of our code, we simulate the photonic crystal slab cavity and calculate the confined electromagnetic field profile of resonant mode (see Fig.1) using three-dimensional FDTD program. All calculation is performed in double-precision [1]. Figure 2 shows the elapsed time of CPU and CPU with GPU for several amount of simulation size. With GPU, our program achieves about 18 times speedup over CPU code. About 2.5 times speedup of GTX 480 over Tesla C1060 can be attributed to the difference in memory band width and L1 cashe.

[1] H. Taniyama et al., PIERS 2011, 1A9-K-14, March (2011).

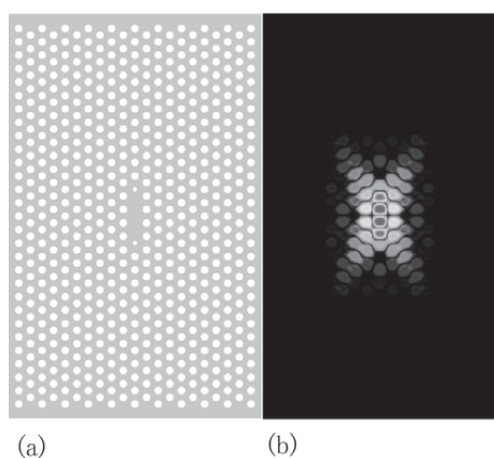


Fig. 1. (a) Photonic Crystal Slab Cavity and (b) field profile of resonant mode.

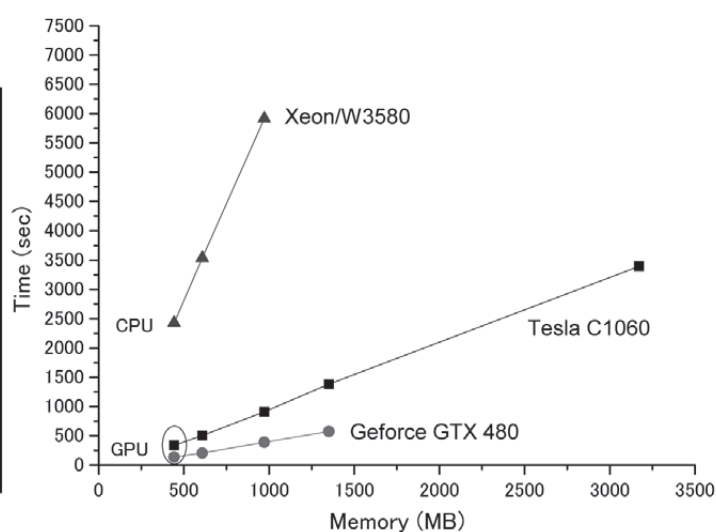


Fig. 2. Elapsed time of FDTD calculation for CPU and CPU with GPU.

II . Data

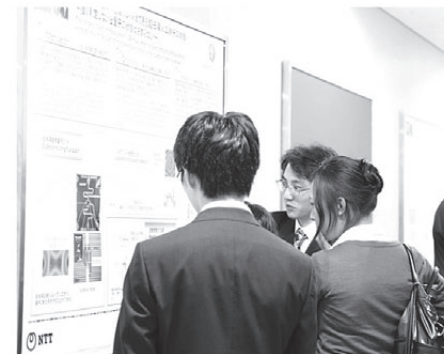
Science Plaza 2010

"Science Plaza 2010," an open-house event of NTT Basic Research Laboratories (BRL), was held at NTT Atsugi R&D Center on Thursday, November 25th, 2010. Under the banner "Frontier Science: Open Door to the Future", Science Plaza aimed to disseminate our latest research accomplishments through various sections of people inside and outside of NTT and to gather diverse opinions.

Following an opening address from Dr. Itaru Yokohama, the director of BRL, one of distinguished technical members of NTT BRL, Dr. Yoshitaka Taniyasu gave a lecture on "Nitride Semiconductor Deep-ultraviolet Light-emitting Diodes – Material Physics and Device Applications". In the afternoon session, Prof. Tatsuo Izawa, Executive Vice President for Research, Tokyo Institute of Technology, gave a special lecture entitled "Optical Fiber Communication and Glass Science". Each lecture was well-attended and followed by heated question-and-answer sessions.

As regards the poster exhibits, 45 posters, including 16 from Microsystem Integration Laboratories, Photonics Laboratories and Communication Science Laboratories, presented our latest research accomplishments. While explaining the originality and impact—as well as the future prospects—of our research accomplishments, these posters were intensively discussed, and many meaningful opinions were heard. This year's "Lab Tour"—a guided tour of research facilities at NTT BRL that has been receiving high reputation from visitors over the years—took place at five different labs, so that as many people as possible could join the tour. This time we also opened a booth to show the NTT R&D recruitment system for job-seeking researchers and students. After all lectures, presentations, and exhibitions, a banquet was held in Center's dining room, where lively conversation among participants deepened their amity.

More than 240 people from research institutes, universities, and general industries, as well as from NTT Group, attended Science Plaza 2010. Thanks to the efforts of all participants, the conference ended on a high note. We would thus like sincerely to express our gratitude to all of the participants.



International Symposium on Nanoscale Transport and Technology (ISNTT2011)

The symposium was held at the NTT Atsugi R&D Center from January 11 to 14, 2011. The carrier transport properties in nanoscale semiconductor and superconducting structures are receiving strong interest due to the potential they offer for novel devices such as solid-state quantum computers, single-electron transistors, nanomechanical systems and spintronic devices and are being extensively studied in many research institutes. To further enhance these studies, this symposium was organized by Dr. Hiroshi Yamaguchi, Dr. Kouichi Semba and Dr. Tatsushi Akazaki of NTT Basic Research Laboratories. NTT Basic Research Laboratories is a leader in these fields and the symposium aspired to gather leading scientists in these fields to discuss the most recent topics.

On the 11th, after opening and welcoming remarks by Dr. Itaru Yokohama (Director of NTT Basic Research Laboratories), Prof. Charles Marcus (Harvard University) gave a plenary lecture on spin manipulation of electrons and nuclei in semiconductor nanostructures. In addition, there were 6 invited and 4 oral presentations on nanomechanics, single-electron systems and superconducting qubits followed by 33 poster presentations in the evening.

On the 12th, 7 invited and 8 oral presentations discussed graphene, single atom devices, coherent transport and the quantum Hall effect, as well as mesoscopic superconductors. These were followed by further 35 poster presentations.

On the 13th and 14th, there were 10 invited and 15 oral presentations on nanomechanics, superconducting qubits, semiconductor quantum dots and qubits, nano-SQUID and spintronics, edge channel, as well as their optical properties.

In total there were 193 participants (including 82 from NTT) who all greatly enjoyed the high-quality presentations and discussions on carrier interactions and spintronics.

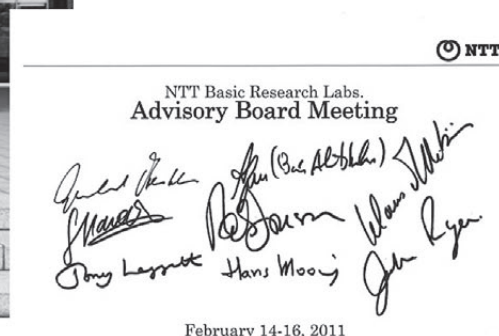
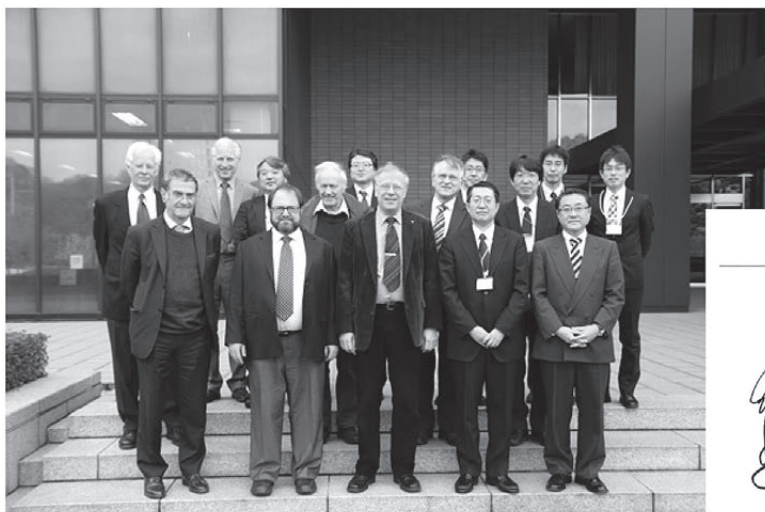


The 6th Advisory Board (Fiscal 2010)

The Advisory Board, an external committee whose role is to evaluate the work of NTT Basic Research Laboratories (NTT-BRL), met from February 14 - 16, 2011. This was the sixth meeting of the Advisory Board, which was first convened in 2001 to provide an objective evaluation of our research plans and activities to enable us to employ strategic management in a timely manner.

Over the course of the three days the board made valuable suggestions and comments in relation to our research and management activities. They commented that the research level is generally high on an international scale, and that it is important for us to maintain this top-level research and transmit information about our research achievements to the world. They also raised several issues related to human resources, the research budget and internal and external collaboration. We plan to make improvements based on these valuable suggestions.

At this meeting, the NTT-BRL researchers had a lunch with the board members and a poster session, where they had chances to present their researches to the board members. The poster session was followed by a dinner party where the board members and the NTT-BRL researchers were able to interact in a casual atmosphere. For the NTT-BRL and NTT executives, we organized a Japanese style dinner, which provided a good chance to discuss the future management strategy of NTT-BRL from an international perspective. The next board meeting will be held in two years.



Board Members

Prof. Abstreiter
 Prof. Altshuler
 Prof. Hänsch
 Prof. Haroche
 Prof. Jonson
 Prof. Leggett
 Prof. Mooij
 Prof. Ryan
 Prof. von Klitzing

Affiliation

Walter Shottky Inst.
 Columbia Univ.
 Max-Planck-Inst.
 Ecole Normale
 Göteborg Univ.
 Univ. Illinois
 Delft Univ. Tech.
 Univ. Oxford
 Max-Planck-Inst.

Research Field

Low-dim. physics
 Condensed matter
 Quantum optics
 Quantum optics
 Condensed matter
 Quantum physics
 Quantum computer
 Nano-bio technology
 Semiconductor physics

Award Winners' List (Fiscal 2010)

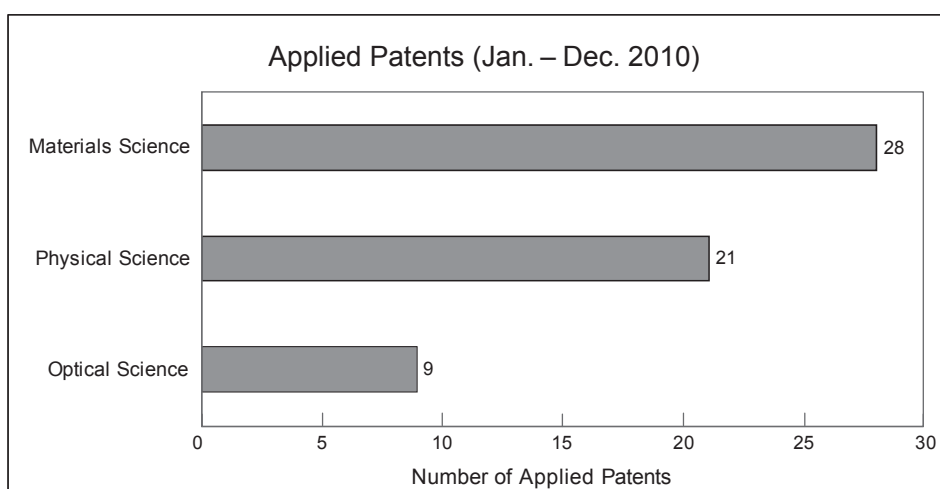
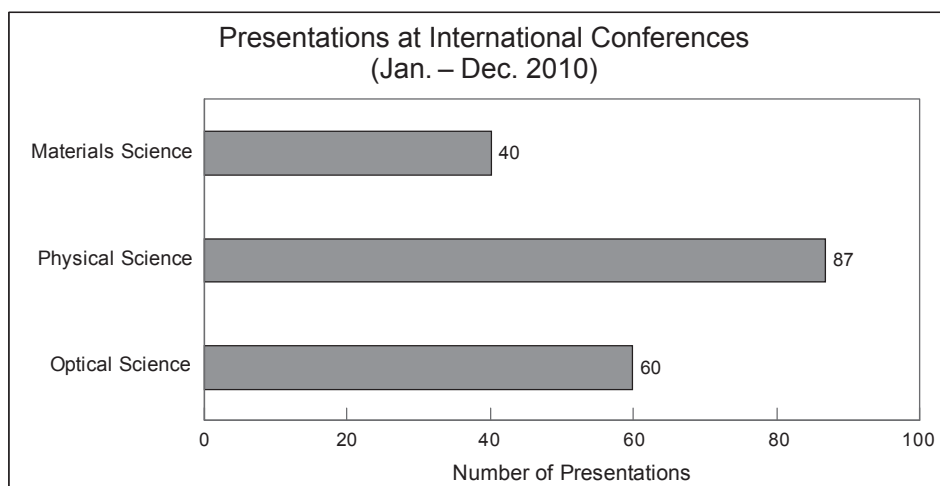
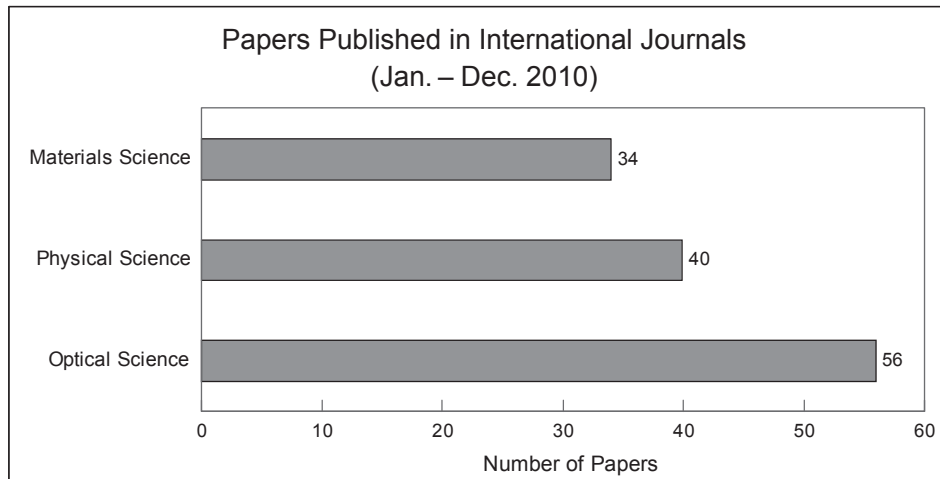
The Science and Technology Award, Commendation by the Minister of Education, Culture, Sports, Science and Technology	M. Notomi	Research on Novel Ways of Controlling Propagation and Confinement of Light by Photonic Crystals	Apr. 13, 2010
The Commendation for Science and Technology by the Minister of Education, Culture, Sports, Science and Technology, The Young Scientists' Prize	H. Takesue	Research on High-speed, Long-distance Quantum Cryptography in Telecommunication Band	Apr. 13, 2010
JSPS Nanoprobetechnology Encouraging Award	Y. Shinozaki	Observation of Structural Dynamics in Single Receptor Proteins with Fast-scanning AFM	Aug. 4, 2010
The 19th International Conference on the Application of High Magnetic Fields in Semiconductor Physics and Nanotechnology (HMF-19): Best Poster Award for Young Researchers	K. Takase	Density-imbalance Stability Diagram of the $\nu_T=1$ Bilayer Electron System at Full Spin Polarization	Aug. 6, 2010
The 27th Paper Award of the Japanese Association for Crystal Growth (JACG)	M. Kasu	Surface Growth Kinetics of Metalorganic Vapor Phase Epitaxy and its Application to High Efficient Aluminum Nitride Devices	Aug. 8, 2010
The Japan Society of Applied Physics Outstanding Paper Award 2010	H. Okamoto D. Ito K. Onomitsu T. Sogawa H. Yamaguchi	Controlling Quality Factor in Micromechanical Resonators by Carrier Excitation	Sep. 14, 2010
JSAP Outstanding Paper Award — 2010	Y. Hayashi K. Tanaka T. Akazaki M. Jo H. Kumano I. Suemune	Superconductor-based Light Emitting Diode: Demonstration of Role of Cooper Pairs in Radiative Recombination Processes	Sep. 14, 2010
International Conference on Solid State Devices and Materials Paper Award	H. Okamoto D. Ito K. Onomitsu H. Sanada H. Gotoh T. Sogawa H. Yamaguchi	Carrier-induced Dynamic Backaction in GaAs Micromechanical Resonators	Sep. 22, 2010
The 24th Diamond Symposium Best Poster Award	K. Hirama	Single-crystal n-type AlN/p-type Diamond Heterojunction Diodes	Nov. 18, 2010

In-house Award Winners' List (Fiscal 2010)

NTT Science and Core Technology Laboratory Group Director Award	S. Matsuo K. Nozaki A. Shinya T. Sato Y. Kawaguchi H. Taniyama T. Tanabe T. Kakitsuka C. H. Chen M. Notomi	Development of Extremely-low-power Photonic-crystal Lasers and Switches	Jan. 19, 2011
NTT Science and Core Technology Laboratory Group Director Award	M. Okamoto K. Ebata K. Yamada S. Itabashi F. Maeda	Replacement of Facility in Clean Rooms of the Building 3 and Dismantlement of the SOR	Jan. 19, 2011
BRL Director Award Award for Achievements	H. Hibino H. Kageshima S. Tanabe M. Nagase	Growth and Characterization of Epitaxial Graphene	Mar. 29, 2011
BRL Director Award Award for Achievements	S. Sasaki	Investigation of the Kondo Effect in Quantum Dots	Mar. 29, 2011
BRL Director Award Award for Achievements	T. Honjo K. Tamaki H. Takesue	Contribution to the Tokyo QKD Network Experiment	Mar. 29, 2011
BRL Director Award Award for Distinguished Service	K. Sumitomo F. Maeda	Contribution to Extending Laboratory Space by Scrapping Large Fixed Asset	Mar. 29, 2011
BRL Director Award Award for Excellent Papers	K. Nozaki T. Tanabe A. Shinya S. Matsuo T. Sato H. Taniyama M. Notomi	"Sub-femtojoule All-optical Switching using a Photonic-crystal Nanocavity," <i>Nature Photonics</i> 4 , 477 (2010).	Mar. 29, 2011
BRL Director Award Award for Excellent Papers	H. Nakano S. Saito K. Semba	"Quantum Time Evolution in a Qubit Readout Process with a Josephson Bifurcation Amplifier," <i>Phys. Rev. Lett.</i> 102 , 257003 (2009).	Mar. 29, 2011
BRL Director Award Award for Excellent Papers	K. Inaba M. Yamashita	"Time-of-Flight Imaging Method to Observe Signatures of Antiferromagnetically Ordered States of Fermionic Atoms in an Optical Lattice," <i>Phys. Rev. Lett.</i> 105 , 173002 (2010).	Mar. 29, 2011
BRL Director Award Award for Encouragement	K. Kakuyanagi	Low-intrusion Quantum State Measurement using Josephson Bifurcation Amplifier	Mar. 29, 2011

Numbers of Papers, Presentations and Patents (2010)

The numbers of papers published in international journals, presentations at international conferences and applied patents in year 2010 amounted to 130, 187, and 58, respectively. The numbers for each research area are as follows;



The numbers of research papers published in the major journals are shown below.

Journals	(IF2009*)	Numbers
Applied Physics Letters	3.554	15
Applied Physics Express	2.223	13
Japanese Journal of Applied Physics	1.138	13
Physical Review B	3.475	10
Physical Review Letters	7.328	9
Physical Review A	2.866	5
Optics Express	3.278	3
Nature Photonics	22.869	2
Optics Letters	3.059	2
Reviews of Modern Physics	33.145	1
Reports on Progress in Physics	11.444	1
Carbon	4.504	1
Journal of Physical Chemistry C	4.224	1
Langmuir	3.898	1
Nanotechnology	3.137	1
IEEE Journal of Selected Topics in Quantum Electronics	3.064	1
Biochimica et Biophysica Acta, General Subjects	2.958	1
Nature Communications	-	1

*IF2009: Impact Factor 2009 (Journal Citation Reports,2009)

The average IF2009 for all research papers from NTT Basic Research laboratories is 3.13.

The numbers of presentations in the major conferences are shown below.

Conferences	Numbers
2010 International Conference on Solid State Devices and Materials	13
The 37th International Symposium on Compound Semiconductors	12
30th International Conference on the Physics of Semiconductors	11
Quantum Nanostructures and Spin-related Phenomena	9
23rd International Microprocesses and Nanotechnology Conference	8
Updating Quantum Cryptography and Communications 2010	8
The 6th International Conference on the Physics and Applications of Spin Related Phenomena in Semiconductors	6
16th Internatinal Conference on Molecular Beam Epitaxy	5
CLEO/QELS	5
International Symposium on Physics of Quantum Technology	5
Materials Research Society Meeting	4
Gordon Research Conference	4
The 19th International Conference on High Magnetic Fields in Semiconductor Physics and Nanotechnology	4
10th International Conference on Quantum Communication	3
Adv. Func. 3D control. Quantum Structures	3
European Materials Research Society	3
Photonic and Electromagnetic Crystal Structures 2010	3
The 6th International Workshop on Nano-scale Spectroscopy and Nanotechnology	3
International Symposium on Graphene Devices 2010	3

List of Invited Talks at International Conferences (2010)

I. Materials Science Laboratory

- (1) K. Torimitsu, "Nanobiodevice architecture using receptor protein", International Conference on Nanoscience and Nanotechnology (ICONN 2010), Sydney, Australia (Feb. 2010). (Plenary)
- (2) K. Torimitsu, Y. Shinozaki, N. Kasai, A. Shimada, K. Sumitomo, C. Ramanujan, and J. F. Ryan, "Understanding the structure and functions of receptor proteins", International Conference on Nanoscience and Nanotechnology (ICONN 2010), Sydney, Australia (Feb. 2010).
- (3) H. Hibino, H. Kageshima, and M. Nagase, "In-situ surface electron microscopy observations of growth and etching of epitaxial few-layer graphene on SiC", International Workshop on in situ characterization of near surface processes 2010, Eisenerz, Austria (May 2010).
- (4) K. Torimitsu, Y. Shinozaki, N. Kasai, A. Shimada, and K. Sumitomo, "Receptor protein based nanobio-interface", Asia-Pacific Symposium on Nanobionics, Wollongong, Australia (June 2010).
- (5) K. Torimitsu, Y. Shinozaki, N. Kasai, A. Shimada, K. Sumitomo, and Y. Furukawa, "Analysis of receptor conformation and its functional relations for biomimetic device", International Conferences on Modern Materials & Technologies 2010, Montecatini Terme, Italy (June 2010).
- (6) K. Hirama, Y. Taniyasu, and M. Kasu, "N-type conduction of single-crystal Si-doped AlN (0001) layer grown on diamond (111) substrate", The 37th International Symposium on Compound Semiconductors, Takamatsu, Japan (June 2010).
- (7) K. Torimitsu, Y. Shinozaki, Y. Furukawa, N. Kasai, and K. Sumitomo, "Conformational nanostructure analysis of receptor protein and its application for biomimetic device formation", Gordon Research Conferences, Tilton, U.S.A. (July 2010).
- (8) T. Akasaka, Y. Kobayashi, and M. Kasu, "Step-free GaN hexagons grown by selective-area MOVPE", The 3rd International Symposium on Growth of III-Nitrides, Montpellier, France (July 2010).
- (9) M. Kasu, "Surface kinetics and growth modes in metalorganic chemical vapor deposition (MOCVD) and their applications to aluminum nitride (AlN)", 16th International Conference on Crystal Growth (ICCG-16)/14th International Conference on Vapor Phase Epitaxy (ICVGE-14), Beijing, China (Aug. 2010).
- (10) H. Hibino, "Dynamics of Si surface morphology/Epitaxial graphene growth on SiC surfaces", The 14th International Summer School on Crystal Growth (ISSCG-14), Dalian, China (Aug. 2010).
- (11) Y. Shinozaki, "Dynamic structural changes in single receptor protein observed with fast-scanning atomic force microscopy", 9th International Conference on Non-Contact Atomic Force Microscopy, Ishikawa, Japan (Aug. 2010).
- (12) H. Hibino, "Surface electron microscopy of epitaxial graphene", 2nd International Symposium on the Science and Technology of Epitaxial Graphene, Amelia Island, U.S.A. (Sep. 2010).
- (13) H. Hibino, H. Kageshima, S. Tanabe, and M. Nagase, "Growth, structure, and transport properties of epitaxial graphene on SiC", International Symposium on Graphene Devices 2010, Sendai, Japan (Oct. 2010).
- (14) K. Torimitsu, "Functional analysis of receptor protein for biomimetic device formation - structure and function -", 4th International Symposium on Nanomedicine (ISNM2010), Okazaki, Japan (Nov. 2010).

II. Physical Science Laboratory

- (1) H. Yamaguchi, I. Mahboob, H. Okamoto, and K. Onomitsu, "Micro/nanoelectromechanical systems for advanced semiconductor devices", 2010 International RCIQE/CREST Joint Workshop, Sapporo, Japan (Mar. 2010).
- (2) Y. Ono, A. H. Khalafalla, K. Nishiguchi, and A. Fujiwara, "Single dopant effects in silicon nano transistors", Single Dopant Control (SDC2010), Leiden, Netherlands (Mar. 2010).
- (3) Y. Ono, M. A. H. Khalafalla, K. Nishiguchi, and A. Fujiwara, "Single dopant effects in silicon nano transistors", The 2010 International Symposium on Atom-scale Silicon Hybrid Nanotechnologies for 'More-than-Moore' & 'Beyond CMOS' Era, Southampton, U.K. (Mar. 2010).
- (4) A. Fujiwara, K. Nishiguchi, and Y. Ono, "Single-electron transfer technology using Si nanowire MOSFETs", The 2010 International Symposium on Atom-scale Silicon Hybrid Nanotechnologies for 'More-than-Moore' & 'Beyond CMOS' Era, Southampton, U.K. (Mar. 2010).
- (5) K. Semba, "Manipulation of entanglement in the heterogeneous quantum system", 5th International Workshop on "Advances in Foundations of Quantum Mechanics and Quantum Information with Atoms and Photons" ad memoriam of Carlo Novero & the 3rd Italian Quantum Information Science Conference (V Quantum 2010 & 3rd IQIS2010), Torino, Italy (May 2010).
- (6) H. Yamaguchi, I. Mahboob, H. Okamoto, and K. Onomitsu, "Challenge for electromechanical logic systems using compound semiconductor heterostructure", 2010 Asia-Pacific Workshop on Fundamentals and Applications of Advanced Semiconductor Devices (AWAD2010), Tokyo, Japan (June 2010). (Plenary)
- (7) Y. Okazaki, S. Sasaki, and K. Muraki, "Spin/pseudospin Kondo effect in a capacitively coupled parallel double quantum dot", 30th International Conference on the Physics of Semiconductors (ICPS2010), Seoul, Korea (July 2010).
- (8) H. Yamaguchi, H. Okamoto, Y. Maruta, S. Ishihara, and Y. Hirayama, "Mechanical to electrical energy transduction using a micromechanical 2DES cantilever", 16th International Conference on Molecular Beam Epitaxy (MBE2010), Berlin, Germany (Aug. 2010).
- (9) K. Kanisawa, "Structure of a single hydrogenic defect in a semiconductor quantum well", Gordon Research Conference: Defects in Semiconductors (GRC), New London, U.S.A. (Aug. 2010).
- (10) H. Kageshima, H. Hibino, M. Nagase, Y. Sekine, and H. Yamaguchi, "Theoretical study on functions of graphene", The 2nd International Symposium on Graphene Devices: Technology, Physics, and Modeling (ISGD 2010), Sendai, Japan (Oct. 2010).
- (11) H. Kageshima, "Mechanism of nanochannel formation processes: thermal oxidation of Si nanostructures and graphene formation on SiC", International Conference on Solid-State and Integrated Circuit Technology (ICSICT2010), Shanghai, China (Nov. 2010).
- (12) H. Kageshima, H. Hibino, M. Nagase, Y. Sekine, and H. Yamaguchi, "Theoretical study on growth, structure, and physical properties of graphene on SiC", Japan-Korea Symposium on Surface and Nanostructure 9th (JKSSN9), Sendai, Japan (Nov. 2010).
- (13) T. Yamaguchi, H. Yamaguchi, and T. Iyoda, "Graphoepitaxy of diblock copolymers for lithographic application", 23rd International Microprocesses and Nanotechnology Conference (MNC2010), Fukuoka, Japan (Nov. 2010).

- (14) H. Yamaguchi, "Quantum effects of motion", Japanese-American Frontiers of Science (JAFoS2010), Chiba, Japan (Dec. 2010).
- (15) K. Nishiguchi and A. Fujiwara, "Single-electron applications using nano-wire MOSFETs", 2010 Workshop on Innovative Devices and Systems (WINDS2010), Hawaii, U.S.A. (Dec. 2010).

III. Optical Science Laboratory

- (1) H. Nakano, K. Oguri, and A. Ishizawa, "Dependence of the broadband spectrum of high-order harmonics driven by a few-cycle laser pulse on carrier-envelope phase", 4th Asian Workshop on Generation and Applications of Coherent XUV and X-ray Radiation, Pohang, Korea (Jan. 2010).
- (2) M. Notomi, "Low-power nanophotonic components based on photonic crystals", SPIE Photonics West, San Francisco, U.S.A. (Jan. 2010).
- (3) M. Notomi, "Nonlinear and adiabatic control of light by photonic crystals", 2nd International Conference on Metamaterials, Photonic Crystals and Plasmonics (META'10), Cairo, Egypt (Feb. 2010) (Plenary).
- (4) K. Oguri, T. Okano, T. Nishikawa, and H. Nakano, "Dynamics of femtosecond laser ablation plume studied with ultrafast x-ray absorption fine structure imaging", The International High-Power Laser Ablation Conference, Santa Fe, U.S.A. (Apr. 2010).
- (5) M. Notomi, E. Kuramochi, T. Tanabe, and H. Taniyama, "Manipulating light with photonic crystal nanocavities and their coupled arrays", SPIE Photonics Europe, Brussels, Belgium (Apr. 2010).
- (6) T. Nishikawa, A. Ishizawa, A. Mizudori, H. Takara, H. Nakano, A. Takeda, and M. Koga, "Approach to achieving a wider mode spacing carrier-envelope phase-locked frequency comb at telecommunications wavelength region", The 2th Shanghai Tokyo Advanced Research Symposium on Ultra Intense Laser Science (STAR2), Xiamen, China (May 2010).
- (7) A. Shinya, S. Matsuo, T. Kakizuka, T. Segawa, G. Sato, E. Kawaguchi, and M. Notomi, "Low-power and high-speed operation of ultra-small photonic crystal nanocavity laser based on InGaAsP/InP buried heterostructure", Conference on Lasers and Electro-Optics, San Jose, U.S.A. (May 2010).
- (8) K. Nozaki, T. Tanabe, A. Shinya, S. Matsuo, G. Sato, T. Kakizuka, E. Kuramochi, M. Notomi, and H. Taniyama, "Extremely-low-power nanophotonic devices based on photonic crystals", Photonics in Switching 2010, Monterey, U.S.A. (July 2010).
- (9) M. Notomi, "Photonic crystal for green ICT?", Photonics and Electromagnetic Crystal Structures (PECS IX), Granada, Spain (Sep. 2010).
- (10) T. Honjo, H. Takesue, and Y. Tokura, "Quantum key distribution/communication research in NTT", Updating Quantum Cryptography and Communication (UQCC) 2010, Tokyo, Japan (Oct. 2010).
- (11) W. Munro, "Scalable quantum repeaters and quantum networks", Updating Quantum Cryptography and Communication (UQCC) 2010, Tokyo, Japan (Oct. 2010).
- (12) H. Nakano, K. Oguri, A. Ishizawa, and T. Nishikawa, "Ultrafast time-resolved spectroscopy using x-ray pulses driven by femtosecond laser pulses", 6th Asian Symposium on Intense Laser Science (ASILS 6), Beijing, China (Oct. 2010).

- (13) K. Tateno, G. Zhang, H. Gotoh, and T. Sogawa, "Characterization of quantum dots in III-V semiconductor nanowires", 6th International Workshop on Nano-Scale Spectroscopy & Nanotechnology (NSS6), Kobe, Japan (Oct. 2010).
- (14) H. Takesue, "Single-photon frequency downconversion experiment", Photonics Global, Singapore, Singapore (Dec. 2010).
- (15) H. Nakano, K. Oguri, A. Ishizawa, and T. Nishikawa, "High-order harmonics of carrier-envelope phase controlled few-cycle laser pulse for probing dynamics of photo-excited solid surface", International Symposium on Ultrafast Intense Laser Science, Hawaii, U.S.A. (Dec. 2010).

**Research Activities in NTT-BRL
Editorial Committee**

NTT Basic Research Laboratories

3-1 Morinosato Wakamiya, Atsugi

Kanagawa, 243-0198 Japan

URL: <http://www.brl.ntt.co.jp/>